Excitation transfer in disordered two-dimensional and anisotropic three-dimensional systems: Effects of spatial geometry on time-resolved observables

J. Baumann[a] and M. D. Fayer
Department of Chemistry, Stanford University, Stanford, California 94305

(Received 31 March 1986; accepted 5 June 1986)

A unified treatment of dipole–dipole excitation transfer in disordered systems is presented for the cases of direct trapping (DT) in two-component systems and donor–donor transfer (DD) in one-component systems. Using the two-particle model proposed by Huber we calculate the configurational average of $G^s(t)$, the probability of finding an initially excited molecule still excited at time t. For the isotropic three-dimensional case treated by Huber excellent correspondence is found with the previously reported infinite diagrammatic approximation. The anisotropy of the dipole–dipole interaction is included in the averaging procedure. Two regimes of orientational mobility are considered: the dynamic and static limit, rotations being much faster or slower, respectively, than the energy transfer. The following geometrical distributions are investigated: (a) Infinite systems of one, two, and three dimensions which lead to Förster-like decays. Two orientational distributions are considered for monolayers: dipoles confined to the plane or oriented isotropically. (b) Bilayers and multilayers. The averaging procedure for transfer from one layer to another is outlined in detail. The main parameters determining the decay of $G^s(t)$ are the surface concentration and the ratio of the layer separation and the Förster radius. In a stack with a small number of layers, which is a finite system in one of the dimensions, an average over positions of the initially excited donor is included. At low surface concentration the decay gradually changes from two- to three-dimensional character as one increases the number of layers. This fractal-like behavior is solely due to the presence of excluded volumes and the finite nature of the system. Experimental observables are considered in detail. An analysis including a general formalism is presented to determine the loss of polarization memory if an excitation is transferred to a random distribution within the given geometrical constraints. It follows that after one transfer step, in the worst case, less than 10% of the initial anisotropy is conserved if the appropriate observation geometry is chosen. The anisotropy decay, which is manifested in a transient grating or fluorescence depolarization experiment, is thus a useful observable for $G^s(t)$ in DD transfer.

I. INTRODUCTION

Since the pioneering work of Förster[1–3] the phenomenon of energy transfer between an excited donor and a suitable acceptor molecule has been studied intensively for a variety of chemical systems in different geometrical arrangements. This broad interest can be attributed to two facts: first, because the transfer probability strongly depends on the separation and relative orientation of the donor and acceptor, energy transfer can serve as a tool to investigate distance and orientation parameters of the systems studied. In order to use energy transfer as a probe of structure, the excited state coupling mechanism and the nature of the spatial distribution of the molecules must be known. Second, energy transfer in the photosynthetic unit is a key step in solar energy conversion in nature[4]; if one wants to be able to mimic nature's light harvesting device in artificial systems, clearly the dynamics of energy transfer and the influence of structural factors must be understood and controlled. While a mass of experiments has been performed under steady-state conditions using fluorescence quantum yields and anisotropy as observables, time-resolved measurements became possible only during the last decade through the development of picosecond resolving instrumentation. It is clear that more information can be extracted from a time-resolved decay curve than from the single data point of a corresponding steady-state result.

One usually encounters two different experimental situations: In a one-component system excitation energy is transferred among molecules of the same kind, provided that they show some overlap between the absorption and emission spectrum. This situation will be referred to as the donor–donor (DD) transfer case. If, on the other hand, trapping centers are introduced, an excitation can migrate among donors and finally become trapped on a trap. A limiting realization of such a system is for low donor concentration so that the energy transfers in a direct step from the donor to an acceptor. This situation, which has been the most thoroughly studied in the past, is known as the direct trapping (DT) case.

The general theoretical treatment of incoherent excitation transfer in disordered systems is a matter of considerable complexity. The early derivations[1–3,5] all investigated

[a] Present address: Institute for Inorganic and Physical Chemistry, Freiestrasse 3, CH-3000 Bern 9, Switzerland.

 0021-9606/86/194087-21$02.10

the direct trapping case, whereas the donor–donor problem was only recently addressed in detail by Haan and Zwanzig.[6] Using a truncated density expansion in Fourier–Laplace space they were able to approximately calculate the average density of excitations at a position r at time t, $G(r,t)$. Based on this method sophisticated approximate solutions have been found using a self-consistent diagrammatic series. Donor–donor transfer[7,8] as well as the general trapping case[9,10] in infinitely extended three-dimensional systems has been treated this way and excellent correspondence to picosecond fluorescence experiments was found over a range of concentrations and times using the diagrammatic approximation. In addition it was demonstrated that the Green's function can be split into three parts: $G^s(t)$, the probability of an excitation being on the initially excited molecule; $G^D(t,r)$, the probability that it is in the donor ensemble; $G^T(t,r)$, the probability of finding it in the ensemble of traps.

The diagrammatic procedure was later adapted to infinite one- and two-dimensional systems.[11] Stepping towards molecular arrangements of finite size the problem of excited state transport in a sphere was attacked theoretically for direct trapping, where an exact solution was obtained, and for donor–donor transfer, where the Green's function could be represented as a truncated power series and a Padé approximant.[12] The theory was able to accurately reproduce the shape of the fluorescence anisotropy decay of dye molecules confined to the surface of a micelle, and from the single adjustable parameter, the micelle radius was obtained.[13] Another type of finite system is an isolated polymer coil; work devoted to extracting the radius of gyration in polymer blends from time-dependent polarized fluorescence experiments is in progress.[14,15]

$G^s(t)$, the configuration averaged probability that the excitation is on the initially excited donor (either because it has not transferred away or because it has left and returned), is a useful part of the full Green's function describing energy transport, which is easily identified with the following observables: in direct trapping, $G^s(t)\cdot e^{-t/\tau}$ is equal to the fluorescence decay of the donor where τ is the fluorescence lifetime in the absence of traps; in donor–donor transfer it is well approximated by the decay of the polarization anisotropy following polarized excitation of the system. This arises from the fact that excitations are transferred from a photoselected ensemble of molecules to a randomly oriented distribution resulting in almost complete depolarization of the fluorescence emitted from molecules not initially excited. The validity of this assumption will be demonstrated in Sec. V. It follows that donor–donor transfer can be examined if the rotational reorientation of the molecules, which also causes depolarization, is slow compared to the time scale of energy transfer; this restriction need not be made for direct-trapping experiments.

Although the quality of the above-mentioned theoretical approaches is impressive as evidenced by their close agreement with the experimental results, their application is limited because of the mathematical complexity. For the case of a random three-dimensional system the inverse Laplace transform, necessary for comparison to experiment, has recently been found.[16] The other situations require numerical inversion. For more complicated geometrical distributions it is essential to have an energy transfer model which is mathematically more tractable and, if possible, can be analytically handled in the time domain. Because we can compare any new approach to the established theories, the new method can be tested. Such an approach has been proposed by Huber *et al.*[17] for donor–donor transfer and by Blumen and Manz[18] for direct trapping. Briefly, the model considers only the interaction between pairs of molecules. An exact configuration averaging leads to a power series, in the trap concentration for direct trapping and in the donor concentration for donor–donor transfer, which is truncated to first order. The result is identical to Förster-type equations for DT and is approximate for DD transfer in the sense that all paths requiring more than two molecules for an excitation to return to the original molecule are excluded. The very appealing feature of this approach is that both the DT and DD case can be treated in a unified way, leading to a general result which distinguishes between the two cases simply by a scaling factor. All investigations, which were concerned with DT only, can therefore be applied in a straightforward way to the DD problem also. Apart from this unification, it is our aim to apply the model to energy transfer in bi- and multilayer systems which are currently being actively investigated.[19,20]

Before doing so, we feel it to be appropriate to review the model and averaging procedure in some detail in Sec. II and to derive results for isotropic, extended systems of one and two dimensions, and review and unify the results for three dimensions in Sec. III. The appropriate equations for the analysis of energy transfer experiments on monolayers follow directly and an interesting application will be discussed, allowing measurement of thickness changes of, for example, films by means of energy transfer. In Sec. IV bi- and multilayers will be considered. Apart from the significance in biophysical investigations and possible applications in solar energy conversion, this arrangement can, in a purely theoretical way, be used to study the effect of restricted geometries on the energy transfer observables. A stack of an infinite number of layers can be viewed as being continuous and random in two dimensions but discrete in the third one. It will be shown under what conditions the discreteness manifests itself.

With respect to rotational motion we restrict ourselves to the two limiting cases of static averaging, where the molecular orientation is fixed on the time scale of the experiment, and dynamic averaging, where a molecule samples all relative orientations in a time much shorter than one energy transfer step. An extension to the intermediate case has been given by Knoester and van Himbergen.[21]

II. THE TWO-PARTICLE MODEL

We will describe the statistics of energy transfer on the basis of an interaction between two molecules, the excited donor and an acceptor for DT, and the excited donor and an unexcited donor for DD transfer, respectively. Let $w(r)$ be the transfer rate where r denotes the separation of the two molecules. The probability $E(t)$ of finding the excitation on the initially excited molecule is, for this isolated pair,

$$E_{DT}(t) = e^{-w(r)t} \tag{2.1}$$

for DT where only the forward transfer is allowed, and

$$E_{DD}(t) = e^{-w(r)t} \cdot \cosh(w(r)t) = \tfrac{1}{2}(1 + e^{-2w(r)t}) \tag{2.2}$$

for DD transfer where a repeated exchange of the excitation is considered. In doing the configurational average we follow the procedure of Blumen[18] and of Huber.[17]

The spatial disorder is modeled by randomly occupying the sites of a lattice with molecules, the excited donor being at the origin. With the probability p that a site is occupied and the assumption that all pairwise interactions between the excited donor and any other molecule are independent, one obtains

$$G^s(t) = \prod_{i=1}^{N} 1 - p + pE_i(t,r_i)\,, \tag{2.3}$$

where the product extends over the N lattice sites. This method of distributing molecules in space automatically excludes all configurations where a site would be occupied by more than one molecule. Expanding the logarithm of Eq. (2.3) in powers of p yields

$$\ln G^s(t) = -\sum_{k=1}^{\infty} \frac{p^k}{k} \sum_{i=1}^{N} [1 - E_i(t,r_i)]^k . \tag{2.4}$$

Next, the summation over sites is replaced by an integration over space, thus going to a continuous spatial distribution $u(r)$, and only the first order term of the series Eq. (2.4) is retained. The probability p becomes a number density ρ in the spatial dimension under consideration. With Eqs. (2.1) and (2.2), Eq. (2.4) is now simplified to

$$\ln G^s_{DT}(t) = -\rho \int_0^{\infty} (1 - e^{-w(r)t}) u(r) dr\,, \tag{2.5a}$$

$$\ln G^s_{DD}(t) = -\frac{\rho}{2} \int_0^{\infty} (1 - e^{-2w(r)t}) u(r) dr\,. \tag{2.5b}$$

A comparison of Eqs. (2.5a) and (2.5b) shows that both equations can be unified by introducing a scaling factor λ:

$$\lambda = 1 \quad \text{for DT}\,, \tag{2.6a}$$

$$\lambda = 2 \quad \text{for DD transfer}\,, \tag{2.6b}$$

$$\ln G^s(t) = -\frac{\rho}{\lambda} \int_0^{\infty} (1 - e^{-\lambda w(r)t}) u(r) dr\,. \tag{2.7}$$

So far we have allowed $w(r)$ to be of any form and have only considered the spatial but not the orientational distribution of the molecules. We restrict further discussion to dipole–dipole coupling which is responsible for the singlet–singlet energy transfer in many organic molecules. The transfer rate is then given by

$$w(r) = \frac{1}{\tau} \frac{3}{2} \kappa^2(\Omega) \left(\frac{R_0}{r}\right)^6, \tag{2.8}$$

where τ is the excited state lifetime in the absence of energy transfer, R_0 the Förster radius, and $\kappa^2(\Omega)$ a dimensionless factor describing the interaction strength of two dipoles as a function of their relative orientation.[3]

In the dynamically averaged limit, denoted by d, one is allowed to average $\kappa^2(\Omega)$ or, equivalently, the transfer rate $w(r)$ over the normalized angular distribution $v(\Omega)$:

$$\langle \kappa^2 \rangle = \int_{\Omega} \kappa^2(\Omega) v(\Omega) d\Omega\,. \tag{2.9}$$

Equation (2.7) now reads

$$\ln G^s_d(t) = -\frac{\rho}{\lambda} \int_0^{\infty} \{1 - \exp[-\lambda \cdot \tfrac{3}{2} \cdot t/\tau (R_0/r)^6 \langle \kappa^2 \rangle]\} u(r) dr\,. \tag{2.10}$$

In the static (st) case, however, the observable itself has to be averaged over the given angular distribution. Adding this integration to the starting Eq. (2.3), one obtains[22]

$$G^s_{st}(t) = \prod_{i=1}^{N} 1 - p + p \int_{\Omega} v(\Omega) E_i(t,r_i,\Omega) d\Omega\,. \tag{2.11}$$

Applying the same set of approximations as before results in

$$\ln G^s_{st}(t) = -\frac{\rho}{\lambda} \int_0^{\infty} \int_{\Omega} \{1 - \exp[-\lambda \cdot \tfrac{3}{2} \cdot t/\tau (R_0/r)^6 \kappa^2(\Omega)]\} \times u(r) dr\, v(\Omega) d\Omega\,. \tag{2.12}$$

The remaining task for any given spatial and angular distribution is to calculate the integrals Eqs. (2.9), (2.10), or (2.12).

An additional degree of complexity is added if the system is of finite size and the distribution $u(r)$ explicitly depends on the position R_D of the excited donor: $u(r;R_D)$. This behavior is found, e.g., if the molecules are distributed within a sphere; yet, as long as the donors are confined to its surface, the donor position is still an invariant of the system. This feature has been used in a recent theoretical investigation on energy transfer in restricted geometries.[37] Clearly, in the absence of positional invariance, an average of the observable over the distribution of donors has to be performed. In the case that there is a finite number of distinct environments (such as positions on a finite chain):

$$G^s(t) = \frac{1}{n} \sum_{i=1}^{n} G^s_i(t)\,, \tag{2.13}$$

where $G^s_i(t)$ is the ensemble averaged decay of an initial excitation located in environment i.

For a continuous donor distribution $\sigma(R_D)$ one integrates

$$G^s(t) = \int_{R_D} G^s(t,R_D) \sigma(R_D) dR_D \tag{2.14}$$

and obtains, by introducing Eq. (2.7) into Eq. (2.14):

$$G^s(t) = \int_{R_D} \sigma(R_D) dR_D \cdot \exp\left[-\frac{\rho}{\lambda} \int_r (1 - e^{-\lambda w(r)t})\, u(r,R_D) dr\right]. \tag{2.15}$$

To simplify this rather unhandy expression one can expand the exponential in the integrand of Eq. (2.15) and truncate to whatever order is felt appropriate:

$$G^s(t) = \int_{R_D} \sigma(R_D) \cdot dR_D \left[1 + \sum_{n=1}^{\infty} \frac{1}{n!} (-J(R_D))^n\right] \tag{2.16}$$

with

$$J(R_D) = \frac{\rho}{\lambda} \int_r (1 - e^{-\lambda w(r) t}) u(r, R_D) dr . \tag{2.17}$$

Making use of the normalization of $\sigma(R_D)$, Eq. (2.16) becomes

$$G^s(t) = 1 + \sum_{n=1}^{\infty} \frac{1}{n!} \int_{R_D} (-J(R_D))^n \sigma(R_D) dR_D . \tag{2.18}$$

Equation (2.18) is generally valid; for the dynamic regime J is given by Eq. (2.17), whereas the static case is obtained if Eq. (2.17) is also averaged with respect to orientations [see for comparison Eq. (2.12)].

III. ISOTROPIC EXTENDED SYSTEMS IN ONE, TWO, AND THREE DIMENSIONS

A. Spatial distribution

We first evaluate the spatial integral of Eqs. (2.10) and (2.12). The distributions $u_\Delta(r)$ in Δ-dimensional space are given by

$$u_1(r) = 2 , \tag{3.1a}$$

$$u_2(r) = 2\pi r , \tag{3.1b}$$

$$u_3(r) = 4\pi r^2 . \tag{3.1c}$$

It is convenient to define a dimensionless concentration c_Δ as the number of molecules within the Δ-dimensional sphere V_Δ of radius R_0:

$$c_\Delta = \rho_\Delta \cdot V_\Delta , \tag{3.2}$$

where

$$V_1 = 2R_0 , \tag{3.3a}$$

$$V_2 = \pi R_0^2 , \tag{3.3b}$$

$$V_3 = \tfrac{4}{3} \pi R_0^3 . \tag{3.3c}$$

With the substitutions

$$\mu = \lambda \frac{3}{2} \frac{t}{\tau} R_0^6 \langle \kappa^2 \rangle \tag{3.4}$$

and

$$y = \frac{\mu}{r^6} , \tag{3.5}$$

one obtains the following simplified integrals for the dynamic case Eq. (2.10): For an infinite line ($\Delta = 1$):

$$\ln G^s_{1d}(t) = -\frac{\rho}{3\lambda} \mu^{1/6} \int_0^\infty (1 - e^{-y}) y^{-7/6} dy . \tag{3.6a}$$

For an infinite plane ($\Delta = 2$):

$$\ln G^s_{2d}(t) = -\frac{\rho}{3\lambda} \pi \mu^{1/3} \int_0^\infty (1 - e^{-y}) y^{-4/3} dy . \tag{3.6b}$$

For an infinite volume ($\Delta = 3$):

$$\ln G^s_{3d}(t) = -\frac{\rho}{3\lambda} 2\pi \mu^{1/2} \int_0^\infty (1 - e^{-y}) y^{-3/2} dy . \tag{3.6c}$$

It is easily found by partial integration that

$$\int_0^\infty (1 - e^{-y}) y^{-\Delta/6 - 1} dy = \frac{6}{\Delta} \Gamma(1 - \Delta/6) , \tag{3.7}$$

where $\Gamma(\alpha)$ is the gamma function.

Combining Eqs. (3.2)–(3.7) one obtains the general result

$$\ln G^s_{\Delta d}(t) = -c_\Delta \lambda^{\Delta/6 - 1} \left(\tfrac{3}{2} \langle \kappa^2 \rangle\right)^{\Delta/6} \Gamma(1 - \Delta/6) \left(\frac{t}{\tau}\right)^{\Delta/6} . \tag{3.8}$$

Proceeding now to the static situation [Eq. (2.12)] we replace the substitution [Eq. (3.4)] by

$$\mu = \lambda \frac{3}{2} \frac{t}{\tau} R_0^6 \kappa^2(\Omega) . \tag{3.9}$$

The spatial integral in Eq. (2.12) follows in the same way as the result [Eq. (3.8)]:

$$\ln G^s_{\Delta st}(t) = -c_\Delta \lambda^{\Delta/6 - 1} \left(\tfrac{3}{2}\right)^{\Delta/6} \cdot \langle |\kappa|^{\Delta/3} \rangle \cdot \Gamma(1 - \Delta/6) \left(\frac{t}{\tau}\right)^{\Delta/6} \tag{3.10}$$

with

$$\langle |\kappa|^{\Delta/3} \rangle = \int_\Omega [\kappa^2(\Omega)]^{\Delta/6} v(\Omega) \, d\Omega . \tag{3.11}$$

It is immediately seen that the dynamic [Eq. (3.8)] and the static [Eq. (3.10)] limit differ only by a scaling factor

$$\gamma = \frac{\langle |\kappa|^{\Delta/3} \rangle}{\langle \kappa^2 \rangle^{\Delta/6}} , \tag{3.12}$$

$$\ln G^s_{\Delta st}(t) = \gamma \cdot \ln G^s_{\Delta d}(t) . \tag{3.13}$$

Equation (3.13) implies that in going from the dynamic to the static situation, the concentration c has to be replaced by $c \cdot \gamma$. This scaling law has been reported before.[8,23] It will be shown that for all situations considered, γ is smaller than 1, so that the decay of $G^s(t)$ is generally slower in the static case. The numerical value of γ depends on both the spatial dimension Δ and the angular distribution $v(\Omega)$, as is seen from Eqs. (2.9), (3.11), and (3.12). It is found by analysis of the above derivation that this concentration scaling only exists if the spatial distribution extends from zero to infinity. If any of the two integration limits differ, which would correspond to a finite size and/or to excluded volumes, the solution of Eqs. (2.10) and (2.12) depends on $\langle \kappa^2 \rangle$ and $\kappa^2(\Omega)$, respectively, in a more complicated way than Eqs. (3.8) and (3.10). An example for this behavior will be found in the bilayers of Sec. IV.

A further general observation can already be made: The functional form of the decay $G^s(t)$ is solely determined by the spatial dimension Δ, governed by the expression $e^{-(t/\tau)^{\Delta/6}}$, while all other parameters discussed so far, c, λ, $\langle \kappa^2 \rangle$, and γ enter only as scaling constants to expand or contract the time scale. It is useful to express this scaling property by incorporating the concentration into the time variable and define

$$\theta_d = c^{6/\Delta} \cdot \frac{t}{\tau} \tag{3.14a}$$

or

$$\theta_{st} = (\gamma c)^{6/\Delta} \cdot \frac{t}{\tau}. \tag{3.14b}$$

On the other hand, this behavior means that the parameters c, $\langle\kappa^2\rangle$, and γ cannot be determined independently from a time-resolved experiment.

B. Orientation

We now consider several angular distribution functions $v(\Omega)$ and calculate the coefficients $\langle\kappa^2\rangle$, $\langle|\kappa|^{\Delta/3}\rangle$, and γ in the spatial dimensions of interest. The orientation factor $\kappa^2(\Omega)$ for dipole–dipole coupling is

$$\kappa^2 = \left[\mathbf{d}_0 \cdot \mathbf{d}_1 - \frac{3}{|\mathbf{r}|^2}(\mathbf{d}_0 \cdot \mathbf{r})(\mathbf{d}_1 \cdot \mathbf{r})\right]^2, \tag{3.15}$$

where $\mathbf{d}_0$, $\mathbf{d}_1$ are unit vectors parallel to dipoles 0 and 1, and $\mathbf{r}$ is the vector joining them. Steinberg[24] gave an elegant expression, reducing the dependence to two angles only:

$$\kappa^2 = \cos^2\psi(3\cos^2\eta + 1), \tag{3.16}$$

where η is the angle between dipole 0 and $\mathbf{r}$ and ψ the angle between dipole 1 and the direction of the electric field at the location of 1, produced by dipole 0. Although the distributions considered here have been covered in the literature, using different approaches, we briefly outline the derivations since the procedure is needed in Sec. IV.

We begin with a random three-dimensional system and allow the dipoles to be oriented isotropically. The angular distribution, using the coordinates of Eq. (3.16) is

$$v(\eta,\psi) = \tfrac{1}{4}\sin\eta\sin\psi. \tag{3.17}$$

With the substitutions

$$x = \cos\psi, \tag{3.18a}$$

$$y = \cos\eta, \tag{3.18b}$$

$\langle\kappa^2\rangle$ is easily expressed as

$$\langle\kappa^2\rangle = \int_0^1 x^2 dx \int_0^1 (3y^2 + 1)\, dy = 2/3. \tag{3.19}$$

This is the result used by Förster.[2] The evaluation of $\langle|\kappa|\rangle$, which describes the static limit, is analogous and the result can be found in Table I.

In proceeding now to a two-dimensional system we consider two different orientational distributions: the dipoles are either isotropically oriented, but still located on a plane, or their directions are confined to lie within the plane but random with respect to the azimuthal angle. We will show that the first case, where the dimensionality of the orientational freedom is higher than the spatial dimension, requires additional considerations and is unique in the series of systems which are discussed in this section. The second distribution, which we refer to as in-plane orientation, is

$$v(\eta,\psi) = \frac{1}{4\pi^2}, \tag{3.20}$$

and therefore

$$\langle\kappa^2\rangle = \frac{1}{4\pi^2}\int_0^{2\pi}\cos^2\psi\, d\psi \int_0^{2\pi}(3\cos^2\eta + 1)\, d\eta = 5/4 \tag{3.21}$$

and

$$\langle|\kappa|\rangle^{2/3} = \frac{1}{4\pi^2}\int_0^{2\pi}(\cos\psi)^{2/3}\, d\psi \times \int_0^{2\pi}(3\cos^2\eta + 1)^{1/3}\, d\eta = 0.9462. \tag{3.22}$$

Equation (3.22) is integrated numerically and the result found identical to the value of Kellerer and Blumen.[25]

Finally we turn to the isotropic orientation, thus allowing the dipoles to be within or to stick out of the plane. In the dynamic limit every excited dipole samples the same distribution of relative orientations to unexcited ones. $\langle\kappa^2\rangle$ therefore has the value 2/3, as in the three-dimensional, isotropic case. In the static limit, however, the mean relative orientation which is seen by an excited dipole depends on its individual direction, more specifically on the polar angle measured from the surface normal. This is easily visualized by comparing a dipole which stands perpendicular to the plane to one which is within the plane. The former lacks all "head-to-head" orientations of the dipoles which are most efficient for energy transfer, while head-to-head orientations are realized for the latter situation. The consequence is that the initial angular distribution w_0 of molecules excited by polarized (or unpolarized) light needs to be included in the orientational average of $|\kappa|^{2/3}$. We consider excitation by polarized light which leads to two distinct excitation profiles: w_{0z} for the electric field perpendicular to the plane and two degenerate distributions w_{0x} and w_{0y} for the field within the plane. Correspondingly we will obtain $\langle|\kappa|^{2/3}\rangle_z$, $\langle|\kappa|^{2/3}\rangle_{xy}$ and, although physically not accessible, the average $\langle|\kappa|^{2/3}\rangle_{\text{uni}}$ if all dipole directions were uniformly excited. The derivation of these averages is given in Appendix A; their values are found

TABLE I. Coefficients in Eqs. (3.8) and (3.10) for some combinations of spatial dimension and angular distribution in infinite systems.

				Dynamic	Static		
Dimension Δ	$\Gamma(1-\Delta/6)$	c_Δ	Angular distribution	$\langle\kappa^2\rangle$	Excitation polarization	$\langle\|\kappa\|^{\Delta/3}\rangle$	γ
3	1.772 45	$\rho_3\frac{4\pi}{3}R_0^3$	isotropic	2/3		0.6901	0.8452
2	1.354 12	$\rho_2\pi R_0^2$	isotropic	2/3	$\perp$ to plane	0.6909	0.7909
					$\parallel$ to plane	0.7641	0.8747
					uniform	0.7397	0.8468
			in-plane	5/4		0.9462	0.8784
1	1.128 79	$\rho_1 2R_0$	isotropic	2/3	uniform	0.8305	0.8886

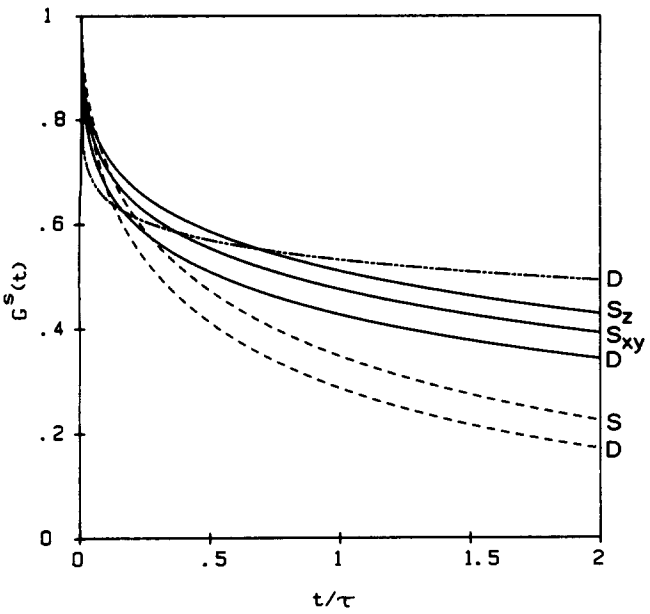

FIG. 1. Decay of $G^s(t)$ for infinite systems of different spatial dimension in the DD transfer situation. The lifetime decay $e^{-t/\tau}$ is not included: Orientation: isotropic; Concentration $c = 1$; (—·—·—) one dimensional; (———) two dimensional; (- - - -) three dimensional; D: dynamic limit; S: static limit; S_z: static limit, excitation polarization normal to the plane; S_{xy}: static limit, excitation polarization in the plane.

in Table I. As expected, $\langle|\kappa|^{2/3}\rangle$ is larger and the decay of $G^s(t)$ therefore faster if the field vector is in the plane, which is the usual experimental situation. The value given by Fredrickson and Frank[23] is based on a uniform excitation profile. It should be noted that even if the light is unpolarized, as long as the field is parallel to the plane, the average $\langle|\kappa|^{2/3}\rangle_{xy}$ has to be used.

All the coefficients needed in Eqs. (3.8) and (3.10) are summarized in Table I. Decay curves $G^s(t)$ for isotropic orientation in all three spatial dimensions are shown in Fig. 1. It is clearly seen that as the spatial dimension becomes lower, the decay is faster at short times and slower at long times. Also in the static isotropic two-dimensional case, the polarization of the excitation field actually influences the rate of energy transport.

C. Validity of the two-particle model

We separately consider the DT and DD results. In the case of DT one realizes that Eq. (3.8) is identical to the expressions derived by Förster[1,2] for $\Delta = 3$ and Hauser *et al.*[28] for $\Delta = 2$ and 1, who use a different procedure to form the configurational average. The fact that the first order term of the exact density expansion [Eq. (2.4)] equals the Förster results is interesting and deserves some comment. While the present method strictly avoids multiple occupation of the same region in space, this possibility is not excluded in the Förster derivation since all molecules are considered independently distributed. This difference is reflected by the presence of higher order density terms in the exact expression [Eq. (2.4)]. Förster-type equations are therefore accurate at low to moderate acceptor concentrations. In order to establish an upper limit for the acceptor concentration, we identify the occupation probability p in the lattice with the fraction f of the total volume occupied by acceptor molecules in the case of a continuous distribution. The first order approximation will be sufficient if p and therefore f are below a maximum value $f_{\max}$. This condition leads to the following upper limits for the concentrations in three- and two-dimensional systems:

$$c_3 \leqslant \frac{4\pi}{3} f_{\max} \frac{R_0^3}{V_{\mathrm{mol}}}, \tag{3.23a}$$

$$c_2 \leqslant \pi f_{\max} \frac{R_0^2}{A_{\mathrm{mol}}}, \tag{3.23b}$$

where V_{mol} and A_{mol} are the molecular volume and area, respectively. A reasonable value for $f_{\max}$ is 0.01, thus reducing the contribution of the second order term to $< 1\%$. Generally, the decay described by Förster-type equations will be faster than the reality because configurations are included which are physically not allowed.

The DD transfer expression ($\lambda = 2$) will now be compared to the infinite order diagrammatic expansion of Gochanour, Andersen, and Fayer (GAF)[7,8] which gave excellent agreement with fluorescence anisotropy decays over a range of concentrations. Knoester and van Himbergen[29] recently made this comparison for four different approaches in three dimensions. After reexpressing the various results as a density expansion they showed that the three-body infinite order GAF approximation is exact up to second order in density. Huber's result, Eq. (3.8), is shown to be exact in first order and its second order coefficient to deviate by only 3% from the exact value. A graphic comparison of the three-body GAF solution and Eq. (3.8) gives two practically indistinguishable curves for concentrations up to $c = 5$ and times which are of significance in experiments. Only the very long-time behavior of $G^s(t)$ is inaccurate as shown by a recent analysis of Fedorenko and Burshtein.[16] This near equivalence to the GAF theory strongly supports the two-particle first order approximation as a valid description for DD transfer even at fairly high concentrations.

For the two- and one-dimensional cases, the three-body infinite order diagrammatic expansions are not available and accurate experimental studies on well-defined systems have only very recently begun to emerge.[32] We therefore have to compare to the two-body infinite order diagrammatic approximation which has been demonstrated to decay somewhat too fast (about 10% at long time) in the three-dimensional case. Therefore, we expect that Eq. (3.8) should decay slower than the two-body theory given by Loring and Fayer[11] for two dimensions. This behavior is indeed found. The decay of the two-dimensional result presented here is slower than the two-body two-dimensional result to essentially the same degree that the three-dimensional three-body result is slower than the corresponding two-body result.

We conclude that in the DT case our equations are equal to Förster-type results; for DD transfer they are an excellent approximation in three dimensions and are expected to be accurate in lower dimensions as well.

D. Applications

1. Monolayers

The preparation of well-defined two-dimensional systems is a rather difficult problem as compared to the three-dimensional counterpart. One way to assemble monomolecular layers is to spread lipids on water under controlled surface pressure and optionally transfer this film onto the surface of a solid substrate.[30] This is known as the Langmuir–Blodgett technique. There are a number of steady-state energy transfer studies in bi- and multilayers.[19,20,33] Yet, to our knowledge, time-resolved experiments concerning energy transfer in an isolated monolayer prepared by the Langmuir–Blodgett technique have not yet been performed. The few picosecond measurements, which have been published, all investigate layers formed by adsorption of molecules from a random solution to the surface of glass, organic crystals, or semiconductors.[31,32] Although these results are encouraging, the accessible range of surface concentrations is limited due to the formation of aggregates at higher concentrations, which act as trapping centers for the excitations. It is to be hoped that these difficulties can be overcome by assembling lipid monolayers, which contain lipophilic chromophores, by the Langmuir–Blodgett technique. It would be valuable to do time-resolved measurements, using the observables outlined in the Introduction, with this type of layer. The interest arises both from the fundamental question on how dimensionality restrictions influence the energy transfer variables and from the potential use of the technique to characterize bi- and multilayers. Independent information about the angular distribution and the time scale of rotational motion, which affect the decay, may be required and can be obtained from polarized fluorescence experiments in diluted systems.[26,27,34]

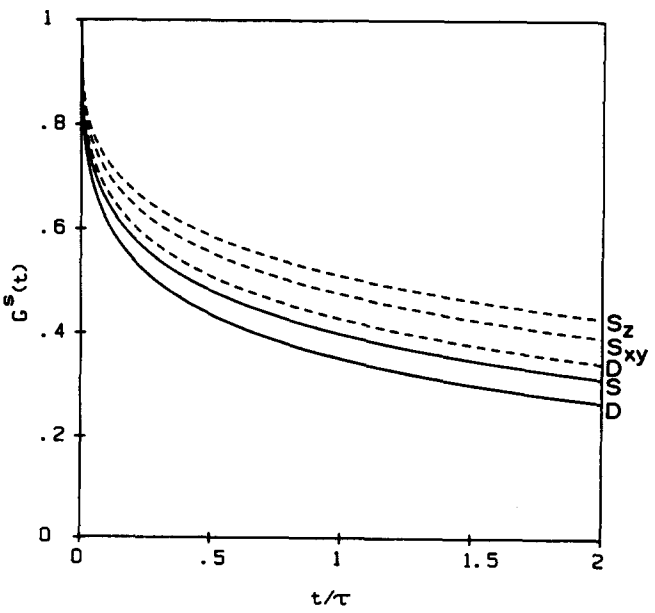

FIG. 2. Decay of $G^s(t)$ for monolayers in the DD transfer situation. Lifetime decay $e^{-t/\tau}$ is not included: Surface concentration $c_2 = 1$; (- - - -) isotropic orientation; (———) in-plane orientation; D, S, S_z, S_{xy} as in Fig. 1.

In Fig. 2 we compare $G^s(t)$ decays for a monolayer in the static and dynamic limit for DD transfer and isotropic as well as in-plane orientation. The curves are calculated from Eqs. (3.8) and (3.10) with $\Delta = 2$ and the coefficients given in Table I. As was pointed out before, the functional form of all curves is the same, the only difference being a scaling of the time axis. The following two features are obvious:

(1) The decay of the statically averaged ensemble is always slower than in the dynamic case.

(2) Isotropic orientation gives rise to a slower decay than the in-plane arrangement. The reason is that in the latter situation relative orientations, which are favorable for energy transfer, are more probable.

It is again interesting to note that for the isotropic case, the polarization of the excitation source influences the rate of energy transfer.

2. Thickness change of films

Consider a film of a thickness large compared to the Förster radius R_0 of chromophores which are randomly distributed in this medium. For example, the film could be a photographic emulsion on a substrate. In such a system, exposure to a solvent results in the film swelling in the direction perpendicular to the plane of the substrate. Energy transfer observables can be used to determine the change of thickness which occurs when a film is swollen by a solvent. Note that the system is modified anisotropically as only one dimension is affected. We will formally show that, although macroscopically an anisotropic change is introduced, the system as a whole still shows exactly isotropic behavior with respect to energy transfer and the expansion factor is easily available from such experiments.

We make the assumption that the orientational distribution and mobility of the molecules do not change. The initial situation is then described by

$$\ln G^s(t) = -\frac{\rho}{\lambda} 4\pi \int_0^\infty (1 - e^{-\mu r^{-6}})\, r^2\, dr\,, \tag{3.24}$$

where μ is the substitution in Eqs. (3.4) or (3.9). After transforming to Cartesian coordinates we obtain

$$\ln G^s(t) = -\frac{\rho}{\lambda} \int_{-\infty}^{\infty}\int_{-\infty}^{\infty}\int_{-\infty}^{\infty} \times\{1 - \exp[-\mu(x^2+y^2+z^2)^{-3}]\}\, dx\, dy\, dz\,. \tag{3.25}$$

We now spatially expand the system anisotropically along the x, y, and z axis by the factors k_x, k_y, and k_z. The only quantity in Eq. (3.25) which is affected by this operation is the density, which is reduced to

$$\rho' = \frac{\rho}{k_x\, k_y\, k_z}\,. \tag{3.26}$$

The integration limits are not influenced because they already extend to infinity. The underlying reason is that we are dealing with a continuous, disordered system which keeps is disorder and continuity even if the macroscopic boundaries are anisotropically changed. $G^s(t)$ is therefore sensitive only to the concentration which is an isotropic quantity.

In contrast, $G^s(t)$ would be affected in a more complicated way if the chromophores formed a lattice. Here, macroscopic anisotropy would result in an anisotropic spatial distribution. To come back to the special case of a film swelling in the x direction only ($k_y = k_z = 1$), we can now give a directly applicable result:

$$\ln G^s(t)_f = \frac{1}{k_x} \ln G^s(t)_i \,, \tag{3.27}$$

where i denotes the initial, f the swollen state. Equation (3.27) holds for the static and dynamic limit. It must be noted that the above argument is only valid if the system is large compared to the distance scale on which energy transfer takes place.

IV. BI- AND MULTILAYERS

Lipid bilayers are widely recognized and used as valuable models for biological membranes. We wish to calculate the energy transfer observables first for a bilayer and then for a stack of any number of monolayers. The procedure which is developed permits the calculation to be carried out for uniformly spaced layers or nonuniformly spaced layers. A multibilayer system is an example of nonuniform spacing. The layer separation in one bilayer is determined by the length of the lipid chains, while the separation between planes of adjacent bilayers is determined by the water content of the multibilayer. For illustration we present specific calculations for a single bilayer and a uniformly spaced stack.

The problem is composed of two parts: transfer from an initially excited donor to a chromophore in the same layer, which has been covered in detail in Sec. III, and transfer to another layer. We will use the terms intralayer and interlayer transfer to distinguish between these two cases. Within the framework of the two-particle approximation, both contributions are independent and can therefore be treated separately. The interlayer contribution could be observed experimentally if the bilayer is prepared such as to contain a small amount of donors on one layer and the acceptors on the other one. If, however, both layers are chemically identical, a combination of intra- and interlayer transfer will be seen in energy transfer experiments.

In the following section we derive the expressions for $G^s(t)$ due to interlayer transfer for isotropic and in-plane orientation, in the dynamic and static limit and taking into consideration the polarization of the exciting light where this is necessary. While in general the configuration average will have to be performed numerically, there exist asymptotic expressions of simple analytic form which are valid if the layer separation is either much smaller or much larger than the Förster radius.

A. Interlayer transfer

The coordinate system used in calculating the interlayer contribution is shown in Fig. 3. d is the separation of the two layers and θ_r denotes the angle between the surface normal and the vector $\mathbf{r}$ which joins the locations of the two dipoles $\mathbf{d}_0$ and $\mathbf{d}_1$. It is convenient to transform the spatial integration of Eqs. (2.10) and (2.12) into an integration over the angle θ_r. We have

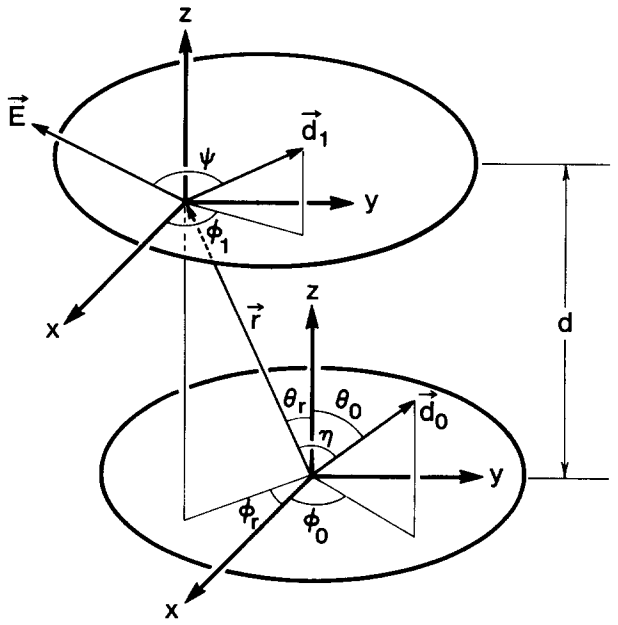

FIG. 3. Coordinate system for interlayer transfer: $\mathbf{d}_0$: donor dipole; $\mathbf{d}_1$: acceptor dipole; E: electric field produced by $\mathbf{d}_0$; d: layer spacing.

$$r = d/\cos\theta_r \,, \tag{4.1}$$

and obtain for the spatial distribution

$$u(\theta_r) = 2\pi d^2 \frac{\sin\theta_r}{\cos^3\theta_r} \,. \tag{4.2}$$

The dynamic case [Eq. (2.10)] is then

$$\ln G_d^s(t) = -\frac{\rho}{\lambda} 2\pi d^2 \int_0^{\pi/2} \left\{ 1 - \exp\left[-\lambda \frac{3}{2} \frac{t}{\tau} (R_0/d)^6 \times \cos^6\theta_r \langle \kappa^2 \rangle \right] \right\} \frac{\sin\theta_r}{\cos^3\theta_r} d\theta_r \,, \tag{4.3}$$

and the static one [Eq. (2.12)]:

$$\ln G_{\rm st}^s(t) = -\frac{\rho}{\lambda} 2\pi d^2 \int_0^{\pi/2} \int_\Omega \left\{ 1 - \exp\left[-\lambda \frac{3}{2} \frac{t}{\tau} (R_0/d)^6 \times \cos^6\theta_r \, \kappa^2(\Omega) \right] \right\} \frac{\sin\theta_r}{\cos^3\theta_r} d\theta_r v(\Omega) \cdot d\Omega \,. \tag{4.4}$$

We introduce the following ratio which will be shown to be a major parameter for the description of interlayer transfer:

$$v = R_0/d \,. \tag{4.5}$$

In addition we define

$$\mu = \frac{3}{2} \lambda \frac{t}{\tau} v^6 \,, \tag{4.6}$$

and the surface concentration

$$c_2 = \rho\pi R_0^2 \,, \tag{4.7}$$

expressed as the number of molecules within a circle of radius R_0.

1. Isotropic orientation

The orientation of the dipoles is assumed to be random in three dimensions, thus allowing them to stick out of the plane on which they are located.

In the dynamic limit, the value of $\langle\kappa^2\rangle$ is 2/3 as found before. From Eq. (4.3), with the substitutions Eqs. (4.5), (4.6), and

$$s=\mu\langle\kappa^2\rangle\cos^6\theta_r \tag{4.8}$$

the following integral is obtained:

$$\ln G_d^s(\mu)=-\frac{c_2}{3\lambda v^2}(\mu\langle\kappa^2\rangle)^{1/3}\int_0^{\mu\langle\kappa^2\rangle}(1-e^{-s})s^{-4/3}\,ds\,. \tag{4.9}$$

The solution is found by partial integration:

$$\ln G_d^s(\mu)=\frac{c_2}{\lambda v^2}\left[1-e^{-\mu\langle\kappa^2\rangle}-(\mu\langle\kappa^2\rangle)^{1/3}\gamma(\tfrac{2}{3},\mu\langle\kappa^2\rangle)\right], \tag{4.10}$$

where γ is the incomplete gamma function:

$$\gamma(\tfrac{2}{3},l)=\int_0^l e^{-s}s^{-1/3}\,ds\,. \tag{4.11}$$

For numerical purposes Eq. (4.11) is most conveniently expressed by its power series[35]

$$l^{1/3}\gamma(\tfrac{2}{3},l)=\sum_{n=0}^{\infty}(-1)^n\frac{l^{n+1}}{(2/3+n)n!}\,. \tag{4.12}$$

It is useful to also derive asymptotic forms for small and large values of μ. If $\mu<0.05$ the integrand of Eq. (4.9) is well approximated by its first order power series:

$$\ln G_d^s(\mu)=-\frac{c_2}{3\lambda v^2}(\mu\langle\kappa^2\rangle)^{1/3}\int_0^{\mu\langle\kappa^2\rangle}s^{-1/3}\,ds\,, \tag{4.13}$$

which yields

$$\ln G_d^s(t)=-\frac{c_2}{2}v^4\frac{t}{\tau},\quad \mu<0.05\,. \tag{4.14}$$

Note that in this limit the decay of $G_d^s(t)$ is exponential and independent of λ; it therefore does not discriminate between the DT and DD transfer situation. This is the time domain where back transfer is still negligible, which is expected at short times or large layer spacing.

In the other extreme $\mu>15$, Eq. (4.10) can be simplified by neglecting the exponential term and approximating the incomplete by the complete gamma function $\Gamma(\frac{2}{3})$:

$$\ln G_d^s(\mu)=\frac{c_2}{\lambda v^2}\left[1-(\mu\langle\kappa^2\rangle)^{1/3}\cdot\Gamma(\tfrac{2}{3})\right]$$
$$=\frac{c_2}{\lambda v^2}(1-1.1829\,\mu^{1/3}),\quad \mu>15\,. \tag{4.15}$$

In the limit of the layers being infinitely close, $\mu\to\infty$, Eq. (4.15) transforms into the equation describing transfer in a monolayer, as given in Eq. (3.8):

$$\lim_{\mu\to\infty}\ln G_d^s(\mu)=-c_2\cdot\lambda^{-2/3}(\tfrac{3}{2}\langle\kappa^2\rangle)^{1/3}\Gamma(\tfrac{2}{3})(t/\tau)^{1/3}\,. \tag{4.16}$$

In the static limit we have to be concerned about the state of polarization of the exciting beam for the same reasons as outlined in the monolayer treatment. The derivation of $\ln G_{\mathrm{st,uni}}^s(\mu)$ for uniform excitation and $\ln G_{\mathrm{st},z}^s(\mu)$ for a polarization perpendicular to the plane is given in Appendix B and summarized below. We make use of Eqs. (A3)–(A5) to express $G_{\mathrm{st},xy}^s(\mu)$ for in-plane polarization by

$$\ln G_{\mathrm{st},xy}^s(\mu)=\tfrac{1}{2}(3\ln G_{\mathrm{st,uni}}^s(\mu)-\ln G_{\mathrm{st},z}^s(\mu))\,, \tag{4.17}$$

where

$$\ln G_{\mathrm{st,uni}}^s(\mu)=\frac{c_2}{\lambda v^2}\int_0^1\int_0^1[1-e^{-q(x,y)}-q(x,y)^{1/3}\times\gamma(2/3,q(x,y))]\,dx\,dy \tag{4.18}$$

and

$$\ln G_{\mathrm{st},z}^s(\mu)=\frac{c_2}{2\lambda v^2}\int_0^1\int_0^1(3y^2-1)\times\sum_{k=1}^{\infty}(-1)^k\frac{q(x,y)^k}{k\cdot k!}\,dx\,dy$$
$$+\frac{3c_2}{2\lambda v^2}\int_0^1\int_0^1(1-y^2)[1-e^{-q(x,y)}-q(x,y)^{1/3}\gamma(\tfrac{2}{3},q(x,y))]\,dx\,dy \tag{4.19}$$

and

$$q(x,y)=\mu x^2(1+3y^2)\,. \tag{4.20}$$

The integrals [Eqs. (4.18) and (4.19)] are evaluated numerically using a Gaussian quadrature algorithm, where the incomplete gamma function is calculated with Eq. (4.12) for $q(x,y)<10$ and approximated by $\Gamma(\frac{2}{3})$ at $q(x,y)>10$. The sum in the first term of Eq. (4.19) converges to

$$\sum_{k=1}^{\infty}(-1)^k\frac{q(x,y)^k}{k\cdot k!}=-C-\ln q(x,y)\quad\text{for } q(x,y)>10\,, \tag{4.21}$$

where C is the Euler constant $C=0.5772$.

The asymptotic forms are

$$\ln G_{\mathrm{st,uni}}^s(t)=-\frac{c_2}{2}v^4\frac{t}{\tau}\quad\text{for } \mu<0.05\,, \tag{4.22}$$

$$\ln G_{\mathrm{st},z}^s(t)=-\tfrac{3}{5}c_2v^4\frac{t}{\tau}\,, \tag{4.23}$$

and

$$\ln G_{\mathrm{st,uni}}^s(\mu)=\frac{c_2}{\lambda v^2}[1-1.0016\,\mu^{1/3}]\quad\text{for } \mu>500\,, \tag{4.24}$$

$$\ln G_{\mathrm{st},z}^s(\mu)=\frac{c_2}{\lambda v^2}[0.8-0.9356\,\mu^{1/3}]\,. \tag{4.25}$$

In order to reduce the time involved in calculation, a table of the integrals in Eqs. (4.18) and (4.19) is generated for a sufficient number of values μ; $\ln G^s(\mu)$ is then easily obtained for any combination of v and t by interpolation in the table.

2. In-plane orientation

For the case of in-plane orientation, the dipoles are randomly oriented within the plane, i.e., each has zero projec-

tion on the normal to the plane. Starting with Eq. (3.15) one obtains for the orientation factor

$$\kappa^2 = [\sin\phi_0 \sin\phi_1 + (1 - 3\sin^2\theta_r)\cos\phi_0 \cos\phi_1]^2 . \tag{4.26}$$

where without loss of generality we have set $\phi_r = 0$. Surprising at first is that κ^2 not only depends on the orientation of the dipoles but also on θ_r. This behavior can be understood by realizing that the dipole–dipole interaction is stronger for a head-to-head orientation than for the "side-to-side" parallel orientation. If the two molecules are directly facing one another ($\theta_r = 0$) the most efficient orientation is the side-to-side, while at large lateral displacement ($\theta_r \to \pi/2$) the head-to-head situation is approached.

The expression Eq. (4.26) can be rearranged into powers of $\cos\theta_r$:

$$\kappa^2 = a_1 - a_2 \cos^2\theta_r + a_3 \cos^4\theta_r \tag{4.27}$$

with

$$a_1 = \tfrac{1}{4}(\cos\Delta + 3\cos\Sigma)^2 , \tag{4.28a}$$

$$a_2 = \tfrac{3}{2}(\cos\Delta + 3\cos\Sigma)(\cos\Delta + \cos\Sigma) , \tag{4.28b}$$

$$a_3 = \tfrac{9}{4}(\cos\Delta + \cos\Sigma)^2 , \tag{4.28c}$$

and

$$\Delta = \phi_0 - \phi_1 , \tag{4.29a}$$

$$\Sigma = \phi_0 + \phi_1 . \tag{4.29b}$$

Starting with the dynamic limit we first need to calculate the average orientation factor

$$\langle\kappa^2\rangle = \langle a_1\rangle - \langle a_2\rangle\cos^2\theta_r + \langle a_3\rangle\cos^4\theta_r . \tag{4.30}$$

These averages are given by

$$\langle a_i\rangle = \frac{1}{4\pi^2}\int_0^{2\pi}\int_0^{2\pi} a_i \, d\phi_0 \, d\phi_1 \tag{4.31}$$

resulting in[36]

$$\langle a_1\rangle = \tfrac{5}{4} , \tag{4.32a}$$

$$\langle a_2\rangle = 3 , \tag{4.32b}$$

$$\langle a_3\rangle = \tfrac{9}{4} . \tag{4.32c}$$

$\langle\kappa^2\rangle$ is recognized to contain the average orientation factor $\frac{5}{4}$ for the monolayer situation, modified by two correction terms which vanish as the monolayer arrangement is approached ($\theta_r \to \pi/2$).

We now insert Eq. (4.30) into Eq. (4.3):

$$\ln G_d^s(\mu) = -\frac{c_2}{3\lambda v^2}\int_0^1 \{1 - \exp[-\mu(\langle a_1\rangle s - \langle a_2\rangle s^{4/3} + \langle a_3\rangle s^{5/3})]\} s^{-4/3} \, ds , \tag{4.33}$$

where

$$s = \cos^6\theta_r . \tag{4.34}$$

The integral in Eq. (4.33) is calculated numerically. Care has to be taken to sample enough points in the proximity of $s = 0$, which is achieved by dividing the range of the integration up into several intervals.

An alternative way to evaluate Eq. (4.33) is shown in Appendix C where also the derivation of the asymptotic forms can be found:

$$\ln G_d^s(t) = -\tfrac{9}{32} c_2 v^4 \frac{t}{\tau} ; \quad \mu < 0.05 , \tag{4.35}$$

$$\ln G_d^s(\mu) = \frac{c_2}{\lambda v^2}(1.8 - 1.4587\,\mu^{1/3} - 0.4974\,\mu^{-1/3}) \quad \text{for } \mu > 5000 . \tag{4.36}$$

The basic equation for the static limit is easily obtained from Eq. (4.33) by performing the angle average of $\ln G^s(\mu)$ instead of the coefficients a_i [Eq. (4.32)]:

$$\ln G_{st}^s(\mu) = -\frac{c_2}{12\lambda v^2\pi^2}\int_0^1\int_0^{2\pi}\int_0^{2\pi} \{1 - \exp[-\mu(a_1 s - a_2 s^{4/3} + a_3 s^{5/3})]\} s^{-4/3} \, ds \, d\phi_0 \, d\phi_1 . \tag{4.37}$$

This triple integration is done numerically by dividing the s interval into several sections. The asymptotic forms are derived in Appendix C:

$$\ln G_{st}^s(t) = -\tfrac{9}{32} c_2 v^4 \frac{t}{\tau} ; \quad \mu < 0.05 , \tag{4.38}$$

$$\ln G_{st}^s(\mu) = \frac{c_2}{\lambda v^2}[1.6 - 1.2813\,\mu^{1/3} + 1.34\cdot\mu^{-1/3}] \quad \text{for } \mu > 5000 . \tag{4.39}$$

3. Results

Before explicitly calculating decay curves for $G^s(t)$ let us summarize the results of the previous section, which was exclusively devoted to the transfer of excitations between layers, i.e., interlayer transfer. In all the five distinct situations of excitation transfer between planes (isotropic/dynamic; isotropic/static/z polarization; isotropic/static/xy polarization; in-plane/dynamic; in-plane/static), we find that $G^s(t)$ decays exponentially if the two layers are far apart as compared to R_0, and the decay constant depends on the specific conditions but not on whether it is a DT or DD transfer experiment. In the other extreme, where the layers are close, the general behavior

$$G^s(t) = r\exp\{-p(t/\tau)^{1/3} - q(t/\tau)^{-1/3}\} \tag{4.40}$$

is found and the parameters r, p, and q are specific to the respective situations. In all cases the monolayer decay is formally obtained if the spacing between the layers approaches zero.

Another way of interpreting the asymptotic forms is to identify large layer spacing with short time and small layer spacing with long-time behavior. This in turn means that, as $G^s(t)$ decays, there is a crossover from the initial exponential to the final $e^{-pt^{1/3} - qt^{-1/3}}$ dependence. Consequently, the scaling of concentration with time, which was demonstrated for infinite systems without excluded volumes in Eq. (3.14), is not found in a bilayer. For the intermediate range between small and large layer separation, we have provided the necessary details to compute tables of the integrals which are involved.

In Figs. 4 and 5 decays of $G^s(t)$ are presented for direct trapping in a bilayer, where the donors are situated in the first layer and the acceptors in the second one. This type of system has been realized and direct-trapping experiments have been carried out under steady-state conditions.[33] In

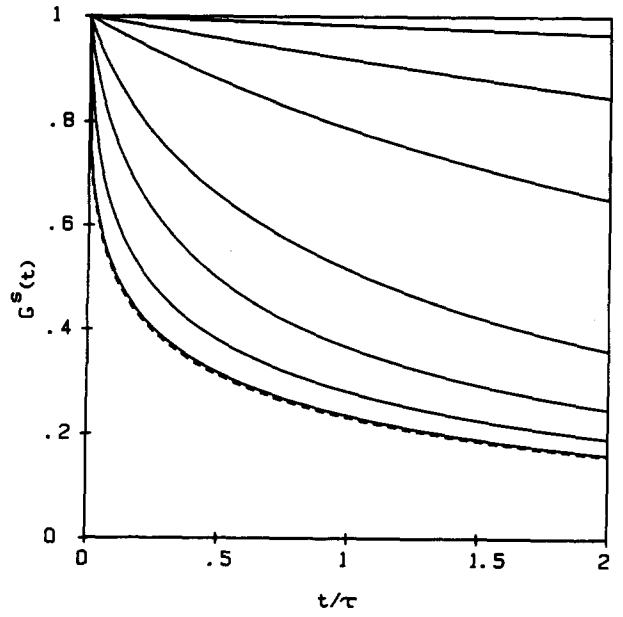

FIG. 4. Decay of $G^s(t)$ in a bilayer for direct trapping in the static limit. Donors are on one layer, acceptors on the other one. Lifetime decay $e^{-t/\tau}$ is not included: Surface concentration of acceptors $c_2 = 1$; Orientation: in-plane; (———) interlayer transfer for $v = R_0/d$, from top to bottom: 0.5, 0.75, 1, 1.5, 2, 3, 10. From Eq. (4.37); (- - - -) intralayer transfer in a monolayer. Donors and acceptors are in the same layer. From Eq. (3.10).

Fig. 4 the orientation is in-plane and the system is taken to be in the static limit. The solid curves differ by the layer spacing d which decreases in going from top to bottom. It is clearly seen that changes in the shape of these decays are most sensitive to the variations of the layer separation if the ratio $v = R_0/d \approx 1$. In experiments designed to measure d, the chromophores should therefore be chosen such that their

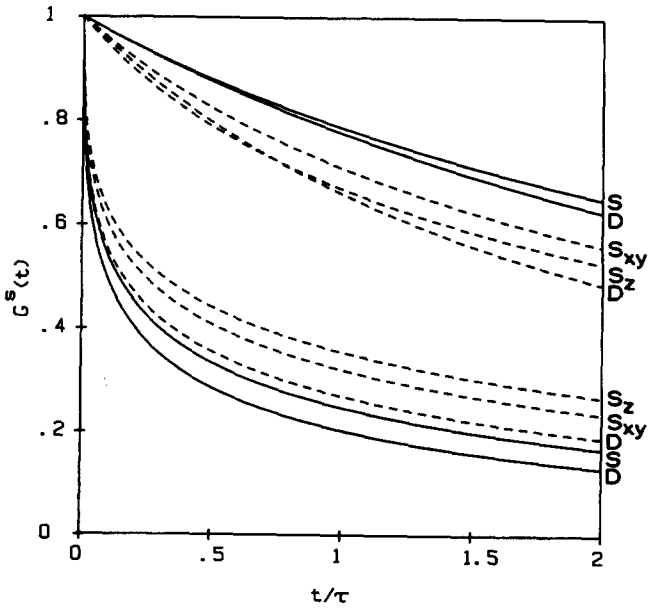

FIG. 5. Decay of $G^s(t)$ in a bilayer for direct trapping; donors are on one layer, acceptors on the other one. Lifetime decay $e^{-t/\tau}$ is not included: Surface concentration of acceptors $c_2 = 1$; R_0/d: 1 for the top 5 curves, 5 for the bottom 5 curves; (- - - -) isotropic orientation; (———) in-plane orientation; D, S, S_z, S_{xy} as in Fig. 1.

Förster radius is comparable to the layer spacing. As the two layers get very close, the transfer observable approaches the form as found in a monolayer which contains both donors and acceptors. This decay is also shown in the figure as a dashed line and one concludes that two layers spaced by less than one-tenth of R_0 are indistinguishable from a monolayer as far as energy transfer is concerned.

In Fig. 5 we examine the effect of the orientational parameters on $G^s(t)$ for direct trapping in the same system as described in Fig. 4. Two different layer spacings are considered: $d = R_0$ and $d = R_0/5$. Figure 5 demonstrates that a precise knowledge of the orientational freedom is required in interpreting this kind of experiment. The decay of an orientationally frozen system is generally slower than its orientationally dynamic counterpart. Interestingly, $G^s(t)$ decays more slowly with in-plane than isotropic orientation if the layers are far apart, while this order is reversed if they are brought together. There is a crossover region which is not shown in the figure.

B. Multilayers

In a stack of n layers, which are chemically equivalent, $G^s(t)$ is composed of the intra- and all possible interlayer contributions. If n is small, the system has to be regarded as finite in the direction normal to the surface. This makes it necessary to average also over starting positions. Since we have positional invariance within the layer, the only spatial variable over which this average is performed is the number of the layer on which the initially excited donor is located. If we denote by $G_i^s(t)$ the probability that an initially excited molecule on the plane i is still excited at time t, the decay for the stack is then given according to Eq. (2.13) by

$$G^s(t) = \frac{1}{n} \sum_{i=1}^{n} G_i^s(t) \,. \tag{4.41}$$

$G_i^s(t)$ is obtained by multiplying the intra- and all interlayer contributions:

$$G_i^s(t) = G_{\text{intra}}^s(t) \prod_{j=1}^{n-i} G_{j,\text{inter}}^s(t) \cdot \prod_{j=1}^{i-1} G_{j,\text{inter}}^s(t) \,, \tag{4.42}$$

where $G_{j,\text{inter}}^s(t)$ denotes interlayer transfer to the jth neighbor layer. The first product in Eq. (4.42) contains the interlayer contributions from layer i to all the layers on one side of i, while the second product is responsible for interlayer transfer on the other side of i. The index j in Eq. (4.42) labels the relative distance of the layer to which energy is transferred from layer i, $j = 1,2,...,$ being the first, second, etc., neighbor layer, respectively.

As n is made large, Eq. (4.42) approaches the expression

$$\lim_{n\to\infty} G_i^s(t) = G^s(t) = G_{\text{intra}}^s(t) \left[\prod_{j=1}^{n/2} G_{j,\text{inter}}^s(t) \right]^2 , \tag{4.43}$$

which is now independent of the starting position i. The numerical procedure used to evaluate Eq. (4.43) is to include

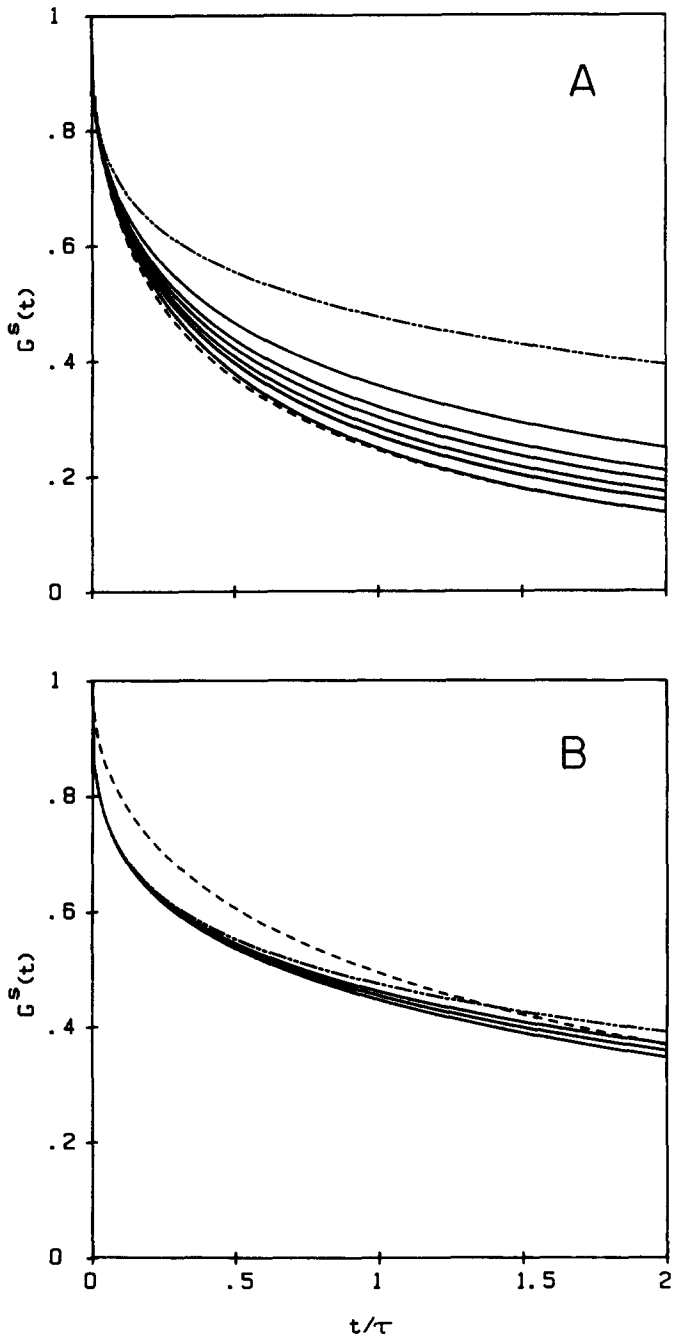

FIG. 6. Decay of $G^s(t)$ in mono-, bi-, and multilayers for DD transfer in the static limit. Lifetime decay $e^{-t/\tau}$ is not included: Surface concentration: $c_2 = 1$; Orientation: isotropic; Excitation polarization: parallel to the layers; (—·—·—) monolayer; (- - - -) random distribution of the same number of molecules in three dimensions. (a) $R_0/d = 1$: (———) multilayer, containing, from top to bottom, 2, 3, 4, 6, 10, ∞ equally spaced layers; (- - - -) equivalent volume concentration $c_3 = \frac{4}{3}$. (b) $R_0/d = 0.5$: (————) multilayer, containing from top to bottom, 2, 4, ∞ equally spaced layers; (- - - -) equivalent volume concentration $c_3 = \frac{2}{3}$.

enough layers for the value of the expression to have converged for all times of interest.

In Fig. 6(a) the overall decay $G^s_{st}(t)$ is shown for a monolayer and stacks of two up to an infinite number of equally spaced layers for DD transfer in the static limit of isotropic orientation. An interesting question to be addressed is to what extent the infinite layer stack behaves differently from a situation where the same number of chromophores is randomly distributed in three-dimensional space. Any difference can be attributed to the fact that a stack of layers has excluded volumes. With the definitions [Eqs. (3.2), (3.3b), and (3.3c)], a volume concentration c_3 can be formally calculated from the surface concentration c_2 of the multilayer system on a purely geometrical basis:

$$c_3 = c_2 \frac{4}{3} \frac{R_0}{d} . \tag{4.44}$$

$G^s(t)$ for the random distribution is then obtained from Eq. (3.10) using c_3 of Eq. (4.44) and is also presented in the figure as a dashed curve. It is obvious that the decay of a stack with infinite layers closely resembles the random solution. Starting from a monolayer we therefore find a gradual transition from two- to three-dimensional behavior as more and more layers are added. However, the validity of this statement depends on the surface concentration.

If in Fig. 6(a) the surface concentration is lowered, the multilayer decay becomes indistinguishable from the random solution over the whole time interval. If the concentration is raised, the decay looks more and more two dimensional. It is reasonable to assume that the ratio p of the mean nearest-neighbor separation in the plane to the layer spacing d is of importance:

$$p = \frac{R_0}{d} \left(\frac{\pi}{c_2} \right)^{1/2} . \tag{4.45}$$

It is found by numerical comparison that for $p > 3$, $G^s(t)$ of the infinite layer stack and the random solution are identical. The intermolecular distances in the plane are on the average larger than the layer separation so that the discreteness of the layered structure is no longer manifested in the energy transfer.

If $p < 1$, the predominant contribution to the overall decay of $G^s(t)$ is intralayer transfer. Adding layers to a monolayer does not change $G^s(t)$, and the decay of the extended stack looks two dimensional. This situation is illustrated in Fig. 6(b).

We therefore conclude that in a multilayer system the decay $G^s(t)$ can vary continuously between the forms for the isotropic two- and three-dimensional cases, depending on the number of layers and the surface concentration. It is tempting to introduce a noninteger spatial dimension into Eqs. (3.8) and (3.10) describing transfer in isotropic systems to account for this behavior. Although we are considering a structure which is by no means fractal,[38] a fractal-like behavior in energy transfer experiments is predicted which is solely due to the presence of excluded volumes and/or the finite character of these structures. A similar conclusion is drawn by Yang *et al.*[39] in a recent paper, where they compare simulations of DT transfer in Vycor glass, which is treated as a regular structure with excluded volumes, to experimental data.

The characteristics of the energy transfer observable in an extended stack illustrated here for DD transfer with isotropic orientation in the static limit, are valid for all other situations as well.

V. EXPERIMENTAL OBSERVABLES

The observable in direct-trapping experiments does not need much comment: it is the decay of the donor fluorescence $I(t)$ which is related to $G^s(t)$ by

$$I(t) = G^s(t) \cdot e^{-t/\tau}, \tag{5.1}$$

where τ is the fluorescence lifetime of the donor in the absence of traps. Alternatively, instead of monitoring time-resolved emission, donor ground state recovery experiments can be performed using either pump-probe or transient grating techniques. [In a transient grating experiment, the signal is proportional to the square of Eq. (5.1).]

In a one-component system the observable for donor–donor transfer is less straightforward. One makes use of the fact that emission from molecules which are excited by polarized light is partially polarized. The observed emission consists of two contributions: the first one originating from the ensemble of initially excited molecules, the second one from those molecules to which energy has been transferred. The usual assumption,[40,41] which has been examined numerically in some detail by Jablonski[42] for isotropic three-dimensional systems, is that there is a sufficient loss of polarization in transferring excitations from the initially excited to the second ensemble that fluorescence from the latter can be treated as completely unpolarized. The experimental observable is the decay of the fluorescence anisotropy or other polarization sensitive observables such as a polarization transient grating. Because we presented in this paper systems of different dimensionalities with respect to spatial and angular distribution, we have to reexamine the above assumption for each situation separately. We will develop a general formalism which permits calculation of the residual anisotropy of the indirectly excited ensemble analytically. We assume that the orientations of the molecules are frozen so that the only process which depolarizes the fluorescence is energy transfer and, for simplicity, that the absorption and emission dipole moments are oriented parallel in the molecular frame. The latter approximation is of importance only if fluorescence anisotropy is measured while it is irrelevant if transient linear dichroism or transient polarization grating[43] experiments are performed to obtain the same information.

In addition, we assume that once an excitation has been transferred it can only return to the molecule it came from but not go to another unexcited molecule. This is equivalent to allowing only pairwise interactions which is the basis of our calculation of $G^s(t)$ in the preceding section. It is clear that this restriction leads to a worst-case estimate because with each additional transfer step to a randomly oriented distribution the remaining polarization memory is reduced further. What we set out to derive is the normalized distribution $w(\Omega;t)$, which is the probability of finding a molecule of orientation Ω excited at time t, including the initially excited and the indirectly excited ensemble after one transfer step, under polarized excitation conditions. We use the term acceptor to denote a molecule which is excited by energy transfer, bearing in mind that donors and acceptors are chemically equivalent.

In order to evaluate $w(\Omega;t)$ we define the following functions: $w_0(\Omega)$ is the initially produced angular distribution of excited molecules. $w_1'(\Omega_0;\Omega)$ is the conditional probability that an excitation from a dipole oriented Ω_0 is transferred to a dipole at Ω, and is determined by averaging the dipole–dipole orientation factor κ^2 [Eqs. (3.15) and (3.16)] for the fixed orientations Ω_0, Ω_1 over spatial configurations. $e^{-t/\tau} \cdot G^s(\Omega;t)$ is the probability of finding an excitation on an initially excited molecule whose orientation is Ω, averaged for spatial configurations and acceptor orientations. $G^s(\Omega;t)$ thus governs the time dependence of transfer from one donor of specified orientation to the whole angular and spatial distribution of acceptors, whereas $w_1'(\Omega_0;\Omega)$ describes how an excitation, which has been transferred, is distributed among acceptor orientations. The distribution $w(\Omega;t)$ can now be expressed if one realizes that $w_0(\Omega)$ disappears with $G^s(\Omega;t)$, while $w_1'(\Omega_0;\Omega)$ builds up with $1 - G^s(\Omega_0;t)$. We therefore obtain

$$w(\Omega;t) = e^{-t/\tau}\Big[w_0(\Omega)G^s(\Omega;t) + \int_{\Omega_0} w_1'(\Omega_0;\Omega) \cdot w_0(\Omega_0) \cdot (1 - G^s(\Omega_0;t)) \cdot v(\Omega_0) \cdot d\Omega_0\Big], \tag{5.2}$$

where $v(\Omega_0)d\Omega_0$ is the angular volume element.

In the case that $G^s(t)$ is independent of the orientation Ω of the excited donor, Eq. (5.2) simplifies to

$$w(\Omega;t) = e^{-t/\tau}\Big[w_0(\Omega)G^s(t) + (1 - G^s(t)) \cdot \int_{\Omega_0} w_1'(\Omega_0;\Omega)w_0(\Omega_0)v(\Omega_0)d\Omega_0\Big]. \tag{5.3}$$

This simplification applies for most systems considered in this paper, except for layers having chromophores with isotropic orientation. Owing to the different ways in which the distributions $w_0(\Omega)$ and $w_1'(\Omega_0;\Omega)$ are created, we apply two distinct coordinate systems, which are compatible with the laboratory fixed coordinates imposed by the polarized fluorescence experiment. Figure 7(a) shows these coordinates used to calculate the initial distribution $w_0(\Omega)$, whereas Fig. 7(b) contains all the angles needed for evaluation of $w_1'(\Omega_0;\Omega)$. The spherical coordinates θ_r and ϕ_r are employed such that the treatment of bilayers is facilitated.

Once the distribution $w(\Omega;t)$ is known, the polarized fluorescence intensities $I_{\parallel}(t)$, $I_{\perp x}(t)$, and $I_{\perp y}(t)$ are obtained in a straightforward way by projecting onto the z, x, and y axis, respectively, and integrating the squared projection over angles:

$$I_{\parallel}(t) = \int_\theta \int_\phi w(\theta,\phi;t)\cos^2\theta v(\theta,\phi)\, d\theta\, d\phi, \tag{5.4a}$$

$$I_{\perp x}(t) = \int_\theta \int_\phi w(\theta,\phi;t)\sin^2\theta\cos^2\phi v(\theta,\phi)\, d\theta\, d\phi, \tag{5.4b}$$

$$I_{\perp y}(t) = \int_\theta \int_\phi w(\theta,\phi;t)\sin^2\theta\sin^2\phi v(\theta,\phi)\, d\theta\, d\phi. \tag{5.4c}$$

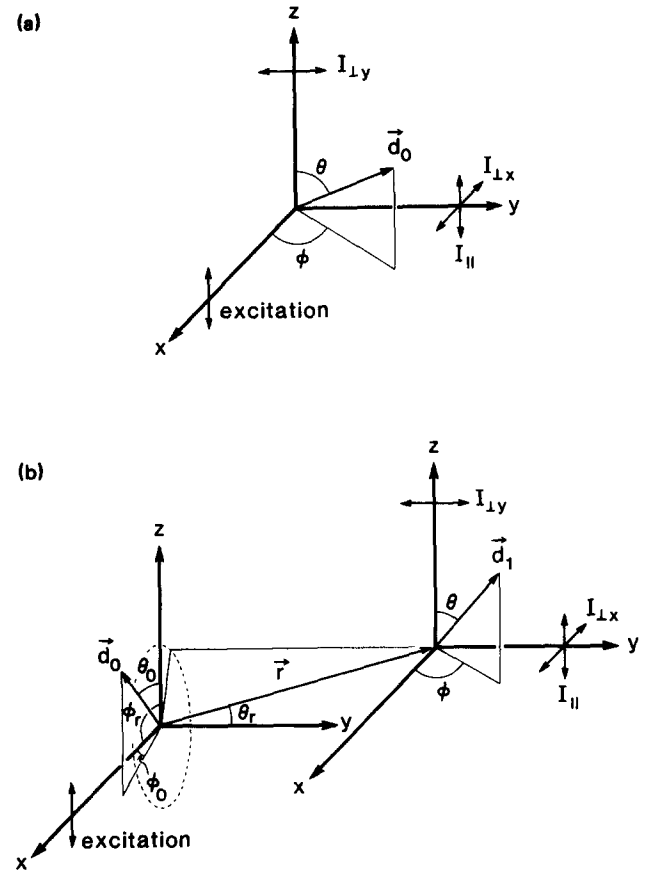

FIG. 7. Coordinate system for polarized fluorescence experiments. Excitation is along the x axis: $I_{\parallel}$: fluorescence intensity polarized parallel to the excitation polarization; $I_{\perp x}$, $I_{\perp y}$: fluorescence intensity polarized perpendicular to the excitation polarization; $\mathbf{d}_0$: directly excited dipole; $\mathbf{d}_1$: dipole excited by one transfer step. (a) Coordinate system for fluorescence from the directly excited ensemble $w_0(\theta,\phi)$. (b) Coordinate system for fluorescence from the indirectly excited ensemble $w_1(\theta,\phi)$ [see Eq. (5.12)].

It will be shown that $I_{\perp x}(t)$ and $_{\perp y}(t)$ are identical in a three-dimensional random distribution. $I_{\perp y}(t)$ will vanish in a layered system with in-plane orientation, and will be found nonzero but different from $I_{\perp x}(t)$ in layers with isotropic orientation. This gives rise to additional considerations concerning the proper conduct of experiments.

The decay of the fluorescence anisotropy, which is the observable to be compared to the theoretical function $G^s(t)$, is in the most general way defined by

$$r_i(t) = \frac{I_{\parallel}(t) - I_{\perp i}(t)}{I_{\parallel}(t) + I_{\perp x}(t) + I_{\perp y}(t)}; \quad i = x, y. \tag{5.5}$$

The remainder of this section is concerned with the evaluation of $w_0(\Omega)$ and the integral in Eq. (5.3) which we denote by

$$w_1(\Omega) = \int_{\Omega_0} w_1'(\Omega_0;\Omega) w_0(\Omega_0) v(\Omega_0)\, d\Omega_0 . \tag{5.6}$$

As stated before, $w_1'(\Omega_0;\Omega)$ is proportional to the orientation factor κ^2 of two interacting dipoles oriented at Ω_0 and Ω, respectively, averaged over spatial configurations and weighted with r^{-6}, the distance dependence for transfer. We therefore have to integrate

$$w_1(\Omega) = \frac{1}{N}\int_{\Omega_0}\int_{\Omega_r} \kappa^2(\Omega_0;\Omega;\Omega_r) \times w_0(\Omega_0) v(\Omega_0) u(\Omega_r) r^{-6}\, d\Omega_0\, d\Omega_r , \tag{5.7}$$

which in the coordinates of Fig. 7(b) becomes

$$w_1(\theta,\phi) = \frac{1}{N}\int_{\theta_0}\int_{\phi_0}\int_{\theta_r}\int_{\phi_r} \kappa^2(\theta_0,\phi_0,\theta,\phi,\theta_r,\phi_r) w_0(\theta_0,\phi_0,) \times v(\theta_0,\phi_0) u(\theta_r,\phi_r) r^{-6}\, d\theta_0\, d\phi_0\, d\theta_r\, d\phi_r . \tag{5.8}$$

N is a normalization constant and $u(\theta_r,\phi_r)$ the spatial distribution of the acceptors. With the same coordinates the orientation factor [Eq. (3.15)] is given by

$$\kappa^2 = [\sin\theta_0 \cos\phi_0 \sin\theta \cos\phi + \sin\theta_0 \sin\phi_0 \sin\theta \sin\phi + \cos\theta_0 \cos\theta - 3(\sin\theta_0 \cos\phi_0 \sin\theta_r \cos\phi_r + \sin\theta_0 \sin\phi_0 \cos\theta_r + \cos\theta_0 \sin\theta_r \sin\phi_r) \times (\sin\theta \cos\phi \sin\theta_r \cos\phi_r + \sin\theta \sin\phi \cos\theta_r + \cos\theta \sin\theta_r \sin\phi_r)]^2 . \tag{5.9}$$

This expression can be inserted into Eq. (5.8) and the quadruple integration carried out analytically for the appropriate spatial distribution $u(\theta_r,\phi_r)$ and the angular distribution $w_0(\theta_0,\phi_0)$ of initially excited molecules, which is a lengthy but straightforward procedure.

In the following sections we present the results for the various geometrical situations which are covered in this work.

A. Isotropic three-dimensional distribution

The normalized initial distribution after polarized excitation as shown in Fig. 7(a) is

$$w_0(\theta,\phi) = 3\cos^2\theta , \tag{5.10}$$

and the angular volume element

$$v(\theta) = \frac{1}{4\pi}\sin\theta . \tag{5.11}$$

For symmetry reasons the distance dependence in Eq. (5.8) is irrelevant here, i.e., transfer from a donor at the origin to acceptors randomly located on a spherical shell will result in an angular distribution $w_1(\theta,\phi)$ whose shape is independent of r; the overall scaling with r^{-6} can be properly accounted for by including it in the normalization factor N. Equation (5.8) thus becomes

$$w_1(\theta,\phi) = \frac{1}{N}\int_0^{\pi}\int_0^{2\pi}\int_0^{\pi}\int_0^{2\pi} \kappa^2 \cdot \cos^2\theta_0 \sin\theta_0 \sin\theta_r \times d\theta_0\, d\phi_0\, d\theta_r\, d\phi_r . \tag{5.12}$$

The result of the integration is

$$w_1(\theta) = \tfrac{3}{25}(8\sin^2\theta + 9\cos^2\theta) . \tag{5.13}$$

As expected, this distribution is axially symmetric and slightly elongated in the direction of the excitation polarization, thus still carrying a small memory of the initial polar-

ization. Inserting Eqs. (5.10) and (5.13) in Eq. (5.3) and projecting according to Eq. (5.4) gives

$$I_{\parallel}(t) = \frac{e^{-t/\tau}}{125}(43 + 32\,G^s(t))\,, \tag{5.14a}$$

$$I_{\perp}(t) = \frac{e^{-t/\tau}}{125}(41 - 16\,G^s(t))\,. \tag{5.14b}$$

The two perpendicular components are identical here. The fluorescence anisotropy Eq. (5.5) is then

$$r(t) = \tfrac{2}{125} + \tfrac{48}{125}\,G^s(t)\,. \tag{5.15}$$

We conclude that the anisotropy decays to a finite value r_∞ at long times, when $G^s(t)$ approaches zero. The ratio of r_∞ to the anisotropy r_0 at $t = 0$ is a measure of the amount of polarization memory which is retained after the first transfer step. One finds from Eq. (5.15) that

$$r_\infty / r_0 = \tfrac{2}{50} = 4\%\,. \tag{5.16}$$

This result is in accordance with the findings of Galanin[40] and Jablonski.[42]

B. Layers with in-plane orientation

We consider only the experimentally realistic case that the excitation polarization is in the plane and the fluorescence is observed along the surface normal. In Fig. 7 the layers are thus in the x–z plane. We start with a monolayer and set

$$\phi_0 = \phi = 0\,, \tag{5.17a}$$

$$\theta_r = \pi/2\,, \tag{5.17b}$$

and

$$v(\theta) = 1/2\pi\,. \tag{5.17c}$$

As in the three-dimensional system, the distance dependence in Eq. (5.8) need not be included.

We have for the initial distribution

$$w_0(\theta) = 2\cos^2\theta \tag{5.18}$$

and

$$w_1(\theta) = \frac{1}{N}\int_0^{2\pi}\int_0^{2\pi} \kappa^2 \cos^2\theta_0\, d\theta_0\, d\phi_r\,, \tag{5.19}$$

which results in

$$w_1(\theta) = \tfrac{1}{20}(19\sin^2\theta + 21\cos^2\theta)\,, \tag{5.20}$$

$$I_{\parallel}(t) = \frac{e^{-t/\tau}}{80}(41 + 19\,G^s(t))\,, \tag{5.21a}$$

$$I_{\perp x}(t) = \frac{e^{-t/\tau}}{80}(39 - 19\,G^s(t))\,, \tag{5.21b}$$

$$I_{\perp y}(t) = 0\,. \tag{5.21c}$$

The anisotropy is

$$r(t) = \tfrac{1}{40} + \tfrac{19}{40}\,G^s(t)\,. \tag{5.22}$$

Again we find a residual anisotropy after long time

$$r_\infty / r_0 = 5\%\,. \tag{5.23}$$

We now turn to a bilayer and make the same analysis for interlayer transfer. $w_0(\theta)$ is the same as (5.18). In contrast to the monolayer, integration over the spatial distribution has to be included in calculating $w_1(\theta)$ and consequently, also the distance dependence. This is deduced from Eqs. (4.27) and (4.28), where it is seen that κ^2 depends on the lateral displacement, expressed by θ_r, between the two dipoles. We make use of Eqs. (4.1) and (4.2) and obtain in analogy to Eq. (5.19):

$$w_1(\theta) = \frac{1}{N}\int_0^{2\pi}\int_0^{\pi/2}\int_0^{2\pi} \kappa^2 \cos^2\theta_0 \sin\theta_r \times \cos^3\theta_r\, d\theta_0\, d\theta_r\, d\phi_r\,. \tag{5.24}$$

The result of this integration is found to be identical to the monolayer case [Eqs. (5.20)–(5.23)]. Energy transfer within the layer or to the next layer, therefore, is detected in the exact same way by means of the anisotropy decay.

C. Layers with isotropic orientation

As has been demonstrated in Secs. III and IV, $G^s(t)$ depends explicitly on the orientation Ω of the initially excited donor, and we have to make use of Eq. (5.2) instead of Eq. (5.3). However, in order to keep the length of this derivation reasonable, we make the assumption that we can average $G^s(t,\Omega)$ over donor angles separately and thus again arrive at the expression [Eq. (5.3)]. $G^s_{\mathrm{st},xy}(t)$, which was calculated in Appendices A, B, and Eq. (4.17) is exactly this average over donor orientations in the case of in-plane polarization. The above approximation can be justified by comparing the decays of $G^s(t)$ for z and in-plane polarization in Figs. 2 and 5, which are seen to be only slightly different. We thus infer that the dependence of $G^s(t,\Omega)$ on the donor orientation Ω is not strong so that using its mean value is a fair approximation. In addition, for $t\to\infty$, Eq. (5.3) becomes exactly identical to Eq. (5.2) since $G^s(t)\to 0$ for all Ω. The residual anisotropy r_∞ which we will obtain using the approximation Eq. (5.3) is thus exact.

We are concerned only with in-plane polarization for situations involving intralayer and interlayer transfer. For a monolayer, which is again oriented in the xz plane of Fig. 7, we set

$$\theta_r = \pi/2\,, \tag{5.25}$$

and neglect the distance dependence in Eq. (5.8). $w_0(\theta)$ and $v(\theta)$ are as defined in Eqs. (5.10) and (5.11).

We have to integrate

$$w_1(\theta,\phi) = \frac{1}{N}\int_0^{\pi}\int_0^{2\pi}\int_0^{2\pi} \kappa^2 \cos^2\theta_0 \sin\theta_0\, d\theta_0\, d\phi_0\, d\phi_r\,, \tag{5.26}$$

which gives

$$w_1(\theta,\phi) = \tfrac{3}{44}(4\sin^2\theta + 15\sin^2\theta\cos^2\phi + 21\cos^2\theta)\,. \tag{5.27}$$

This is the first time we obtain an angular distribution of excited acceptors which is no longer axially symmetric. Consequently, there are two distinctly different perpendicular fluorescence components:

$$I_{\parallel}(t) = \frac{e^{-t/\tau}}{110}(43 + 23\,G^s(t))\,, \tag{5.28a}$$

$$I_{\perp x}(t) = \frac{e^{-t/\tau}}{110}(41 - 19\,G^s(t))\,, \tag{5.28b}$$

$$I_{\perp y}(t) = \frac{e^{-t/\tau}}{110}(26 - 4\,G^s(t))\,, \tag{5.28c}$$

and

$$r_x(t) = \tfrac{1}{55} + \tfrac{21}{55}\,G^s(t)\,, \tag{5.29}$$

$$(r_\infty/r_0)_x = 4.5\%\,, \tag{5.30}$$

$$r_y(t) = \tfrac{17}{110} + \tfrac{27}{110}\,G^s(t)\,, \tag{5.31}$$

$$(r_\infty/r_0)_y = 38.6\%\,. \tag{5.32}$$

A few comments are necessary here: in order to calculate the anisotropy $r_x(t)$ or $r_y(t)$ from polarized fluorescence decays [Eq. (5.5)], all of the three different orthogonal fluorescence components must be measured. In a layer system as discussed here, it is, for obvious reasons, very difficult to obtain $I_{\perp y}(t)$ experimentally. In order to be able to extract the anisotropy one can follow two different lines. The denominator of Eq. (5.5) corresponds to the overall decay $I(t)$ of the molecules, which can be measured in the absence of energy transfer, i.e., at low concentration. Knowing $I(t)$, one can obtain $r_x(t)$ as defined in Eq. (5.5) from two polarized fluorescence decays only:

$$r_x(t) = \frac{I_\parallel(t) - I_{\perp x}(t)}{I(t)}\,. \tag{5.33}$$

The alternative approach is to observe the fluorescence no longer normal to, but at 45° from the surface, in the xy plane. We denote the perpendicular fluorescence component, which one measures in this observation geometry, by

$$I_{\perp xy}(t) = \tfrac{1}{2}(I_{\perp x}(t) + I_{\perp y}(t)) = \frac{e^{-t/\tau}}{220}(67 - 23\,G^s(t))\,. \tag{5.34}$$

The parallel component $I_\parallel(t)$ obtained in this measurement configuration is identical to $I_\parallel(t)$ measured in a rectangular observation geometry. The corresponding anisotropy is then

$$r_{xy}(t) = \frac{I_\parallel(t) - I_{\perp xy}(t)}{I_\parallel(t) + 2I_{\perp xy}(t)} \tag{5.35}$$

and is again experimentally available from two polarized fluorescence decays only. The connection of Eq. (5.35) to $G^s(t)$ is easily obtained from Eqs. (5.28) and (5.34):

$$r_{xy}(t) = \tfrac{19}{220} + \tfrac{69}{220}\,G^s(t)\,, \tag{5.36}$$

$$(r_\infty/r_0)_{xy} = 21.6\%\,. \tag{5.37}$$

This high residual anisotropy is unfortunate and we conclude that the rectangular measurement geometry should be used at the expense of having to measure the sample lifetime independently.

Interlayer transfer in a bilayer follows in an analogous way. We use $w_0(\theta)$ and $v(\theta)$ from Eqs. (5.10) and (5.11), $u(\theta_r)$ from Eq. (4.2), and include the distance dependence to obtain

$$w_1(\theta,\phi) = \frac{1}{N}\int_0^\pi\int_0^{2\pi}\int_0^{\pi/2}\int_0^{2\pi} \kappa^2 \cos^2\theta_0 \sin\theta_0 \sin\theta_r \cos^3\theta_r \cdot d\theta_0\, d\phi_0\, d\theta_r\, d\phi_r\,, \tag{5.38}$$

and after integrating

$$w_1(\theta,\phi) = \tfrac{1}{8}(5\,\sin^2\theta + 7\sin^2\theta\sin^2\phi + 7\cos^2\theta)\,. \tag{5.39}$$

Again this distribution has no axial symmetry. It is interesting to note that there is considerable transfer to dipoles perpendicular to the surface as evidenced by the $\sin^2\phi$ term, although the excitation polarization is within the plane. This behavior is, as discussed earlier, a consequence of the head-to-head alignment of the dipoles being the most efficient for energy transfer. This relative orientation is available only for initially excited dipoles with substantial out-of-plane orientation.

We obtain from Eq. (5.39),

$$I_\parallel(t) = \frac{e^{-t/\tau}}{60}(19 + 17\,G^s(t))\,, \tag{5.40a}$$

$$I_{\perp x}(t) = \frac{e^{-t/\tau}}{60}(17 - 5\,G^s(t))\,, \tag{5.40b}$$

$$I_{\perp y}(t) = \frac{e^{-t/\tau}}{60}(24 - 12\,G^s(t))\,, \tag{5.40c}$$

$$I_{\perp xy}(t) = \frac{e^{-t/\tau}}{120}(41 - 17\,G^s(t))\,, \tag{5.40d}$$

where $I_{\perp xy}$ has been defined in Eq. (5.34).

Going further we find

$$r_x(t) = \tfrac{1}{30} + \tfrac{11}{30}\,G^s(t)\,, \tag{5.41}$$

$$(r_\infty/r_0)_x = 8.3\%\,, \tag{5.42}$$

$$r_y(t) = -\tfrac{1}{12} + \tfrac{29}{60}\,G^s(t)\,, \tag{5.43}$$

$$(r_\infty/r_0)_y = -20.8\%\,, \tag{5.44}$$

and

$$r_{xy}(t) = -\tfrac{1}{40} + \tfrac{17}{40}\,G^s(t)\,, \tag{5.45}$$

$$(r_\infty/r_0)_{xy} = -5.6\%\,. \tag{5.46}$$

The negative values [Eqs. (5.44) and (5.46)] are a direct consequence of the favored transfer to dipoles with out-of-plane orientation.

To decide between rectangular and 45° observation in this case one has to be aware that in the one-component bi- and multilayers intra- and interlayer transfer always occur together. While the 45° geometry is favorable for the interlayer contribution [Eq. (5.46)] it leads to a high residual anisotropy for the intralayer part [Eq. (5.37)]. Under right-angle observation, however, the residual anisotropy of both contributions is well below 10% [Eqs. (5.30) and (5.42)] so that this setup is to be preferred for mono- and multilayers.

D. General remarks

We have proven that there exists a direct relationship between $G^s(t)$ as calculated for DD transfer in the static limit and the decay of the fluorescence anisotropy $r(t)$. In all geometrical situations studied we find that a small anisotropy remains when $G^s(t)$ has decayed to zero.

As demonstrated throughout the paper, the behavior of layered systems which allow isotropic orientation is richer than all the other geometries. We have shown that the three orthogonal fluorescence components in such a system are not identical, which is a direct consequence of the anisotrop-

ic dipole–dipole interaction, and the orientational dimensionality being higher than the spatial one. We have demonstrated how anisotropies have to be calculated from polarized fluorescence measurements and which observation geometry should be chosen to obtain the most reliable data.

In this section we established the relationship between $G^s(t)$ and the fluorescence anisotropy. However, the same information can also be obtained from pump-probe or polarization grating experiments[43] using polarized pump and probe beams. In a pump-probe experiment the observables are the time-dependent transmissions $T_\parallel(t)$, $T_\perp(t)$ of the probe beams polarized parallel and perpendicular to the pump beam. It is easily shown that these transmissions are proportional to the polarized fluorescence intensities $I_\parallel(t)$, $I_\perp(t)$ used so far.

In a polarization grating experiment, two pulses of orthogonal relative polarization are crossed inside the sample to set up a pattern of periodically varying states of polarization. A probe pulse is diffracted off this grating. The decay of the diffracted intensity $D(t)$ is found to be

$$D(t) \propto (I_\parallel(t) - I_\perp(t))^2 = (e^{-t/\tau} \cdot r(t))^2 . \qquad (5.47)$$

Any residual anisotropy will be less prominent in a polarization grating experiment because the square of $r(t)$ is observed. An advantage of this technique is that one measures against a zero background and that the difference $I_\parallel(t) - I_\perp(t)$ results from a single measurement which makes numerical subtraction [Eq. (5.5)] of two independent curves unnecessary. If layered systems with isotropic orientation are to be measured, some care has to be taken to orient the sample in such a way that the plane, which is defined by the two polarization vectors of the excitation beams, coincides with the layers in the sample. This is most easily realized at a small intersection angle of the beams.

VI. CONCLUSIONS

We have described the excitation transfer function $G^s(t)$ in a unified way for either direct-trapping or donor–donor transfer experiments. The general formalism allows for fast or frozen rotational motion of the molecules and for any orientational and spatial distributions. The extension to discrete and continuous systems of finite size has been discussed. We have examined to what accuracy the decay of the fluorescence anisotropy is a measure of $G^s(t)$ in the case of DD transfer. We found that in all situations studied, the residual anisotropy at long times is $< 10\%$ of the initial value after a single transfer step, if the observation geometry is chosen appropriately. In many situations this residual anisotropy is even $< 5\%$. We have derived the general procedure to make these estimates for other systems as well.

The bulk of this work is concerned with the derivation of the configuration average of $G^s(t)$ in several geometrical distributions. We obtained Förster-type analytic expressions for infinite disordered systems. Comparison of the result for a three-dimensional system to the three-body infinite order diagrammatic expansion of GAF[7] established the validity of the two-particle model up to relatively high concentrations.

Transfer on monolayers is seen to depend markedly on the orientational degree of freedom. The behavior is richest if the orientational dimensionality is higher than the spatial one; in this case the polarization of the exciting light relative to the surface influences the decay of $G^s(t)$. In going to bilayers we separated $G^s(t)$ into two independent parts, one accounting for transfer within the layer where the excited donor is located, the other one describing transfer to the other layer. For the interlayer contribution exponential decay is found for large layer spacing while monolayer behavior is approached if the two layers are very close. For the intermediate regime the configuration average has to be obtained numerically which we described in some detail.

Knowing the intra- and interlayer transfer functions, multilayers can be investigated by properly multiplying all the required contributions. An average over starting layers, i.e., the layer on which the initially excited donor is located, has to be performed. It is found that there is a gradual transition from two- to three-dimensional decay behavior as one adds more and more layers to a monolayer, on condition that the mean nearest neighbor distance within the plane is significantly larger than the layer spacing; a stack containing a large number of layers can thus behave almost exactly as a random solution. However, if the layers are drawn apart, thereby leaving the surface concentration unchanged, transfer within the layer dominates and the overall decay is closer to two dimensional. One deduces from the material presented that energy transfer experiments can measure the interlayer distance if the surface concentration and the orientational distribution are known. The procedure can be easily applied to stacks of bilayers which usually possess two different layer spacings. Energy transfer experiments in aligned stacks of phospholipid bilayers containing lipophilic chromophores are in progress in this laboratory.

The two-particle interaction model, averaged over the spatial and angular configurations, has thus proven valuable in gaining insight into energy transfer behavior in a variety of systems. Applications to finite size polymer systems are in progress. It is to be hoped that the approach described here can serve to model energy transfer in many other systems which are of experimental interest.

ACKNOWLEDGMENTS

This work was made possible by support from the Department of Energy, Office of Basic Energy Sciences (Grant No. DE-FG03-84ER13251). We would like to thank R. P. Domingue for many helpful discussions. We would also like to thank Dr. J. L. Lippert, Eastman Kodak Research Laboratories, Rochester, New York, who brought the film swelling problem to our attention. J. B. acknowledges partial support by a fellowship from the Schweizerischer Nationalfonds zur Förderung der Wissenschaftlichen Forschung.

APPENDIX A

In this appendix we derive the average of $|\kappa|^{2/3}$ for a monolayer with isotropic angular freedom for different polarizations of the exciting light.

We first consider the hypothetical situation that there is a uniform excitation probability for all differently oriented

dipoles. In analogy to Eqs. (3.16)–(3.19) we obtain

$$\langle|\kappa|^{2/3}\rangle_{\text{uni}} = \int_0^1 x^{2/3}\,dx \int_0^1 (3y^2+1)^{1/3}\,dy = 0.7397\,. \tag{A1}$$

Let the surface normal be the z axis. If we excite with polarized light, the E field being parallel to the x, y, or z axis, we produce the initial distributions $w_{0,x}$, $w_{0,y}$, and $w_{0,z}$, respectively. Each of them represents a $\cos^2$ distribution which we normalize individually. They add up to the uniform distribution

$$3w_{0,\text{uni}} = w_{0,x} + w_{0,y} + w_{0,z}\,. \tag{A2}$$

The same must be true for the average of any function f, where the average is formed over the initial distribution and all relative orientations to the acceptor dipoles at all positions:

$$3\langle f\rangle_{\text{uni}} = \langle f\rangle_x + \langle f\rangle_y + \langle f\rangle_z\,. \tag{A3}$$

For symmetry reasons we also have

$$\langle f\rangle_x = \langle f\rangle_y\,. \tag{A4}$$

This allows us to use the linear combination

$$\tfrac{1}{2}(w_{0,x} + w_{0,y}) = w_{0,xy}\,, \tag{A5}$$

which is now adapted to the symmetry of the overall spatial distribution. We therefore need to calculate only

$$\langle f\rangle_{xy} = \langle f\rangle_x = \langle f\rangle_y\,, \tag{A6}$$

and obtain $\langle f\rangle_z$ from Eq. (A3) by

$$\langle f\rangle_z = 3\langle f\rangle_{\text{uni}} - 2\langle f\rangle_{xy}\,. \tag{A7}$$

The reason for constructing symmetry adapted distributions is that the average can be performed more easily using the two angles of Eq. (3.16) only, rather than five spherical coordinates: two for the donor orientation, two for the acceptor orientation, and one for the acceptor position. Since both distributions $w_{0,z}$ and $w_{0,xy}$ are axially symmetric we are allowed to fix the position of the acceptor relative to the donor and calculate two types of averages: $\bar{f}_p$ for a $\cos^2$ distribution whose symmetry axis coincides with the vector joining the two dipoles, and $\bar{f}_n$ if they are orthogonal. We denote the former initial distribution by w_{0p} and the latter by w_{0n}. As before there is the additivity relation

$$3\bar{f}_{\text{uni}} = \bar{f}_p + 2\bar{f}_n = 3\langle f\rangle_{\text{uni}}\,. \tag{A8}$$

Note that $\langle f\rangle$ denotes an average over relative orientations and positions, whereas $\bar{f}$ is the orientational average for a fixed relative position.

It is easily seen from the definition of the angles η and ψ in Eq. (3.16) that $\bar{f}_p$ can be calculated using these coordinates:

$$\begin{aligned}\bar{f}_p = \overline{|\kappa_p|^{2/3}} &= \frac{1}{4}\int_0^{\pi} (\cos\psi)^{2/3}\sin\psi\,d\psi \\ &\quad\times \int_0^{\pi} (1+3\cos^2\eta)^{1/3}\cos^2\eta\,d\eta \\ &= \int_0^1 x^{2/3}\,dx \int_0^1 y^2(1+3y^2)^{1/3}\,dy = 0.8373\,.\end{aligned} \tag{A9}$$

$\bar{f}_n$, which is identical to $\langle f\rangle_z$, follows from Eq. (A8):

$$\langle f\rangle_z = \bar{f}_n = \tfrac{1}{2}(3\langle f\rangle_{\text{uni}} - \bar{f}_p) \tag{A10}$$

and

$$\langle f\rangle_{xy} = \tfrac{1}{2}(\bar{f}_p + \bar{f}_n) = \tfrac{1}{4}(3\langle f\rangle_{\text{uni}} + \bar{f}_p)\,. \tag{A11}$$

Combining Eqs. (A1) and (A9)–(A11) for $f = |\kappa|^{2/3}$ yields

$$\langle|\kappa|^{2/3}\rangle_z = 0.6909\,, \tag{A12a}$$

$$\langle|\kappa|^{2/3}\rangle_{xy} = 0.7641\,. \tag{A12b}$$

All integrations were performed numerically.

APPENDIX B

Here we present the derivation of $G^s_{\text{st,uni}}(\mu)$ and $G^s_{\text{st},z}(\mu)$ for interlayer transfer in a bilayer with isotropic orientation, corresponding to uniform and polarized excitation perpendicular to the planes. The coordinate system is shown in Fig. 3.

We start with Eq. (4.4) and obtain for the hypothetical uniform excitation, following the same approach as in the dynamic limit:

$$\begin{aligned}\ln G^s_{\text{st,uni}}(\mu) = \frac{c_2}{\lambda v^2}\int_\Omega [1 - e^{-\mu\kappa^2(\Omega)} \\ - (\mu\kappa^2(\Omega))^{1/3}\gamma(\tfrac{2}{3},\mu\kappa^2(\Omega))] \\ \times v(\Omega)\,d\Omega\,.\end{aligned} \tag{B1}$$

Implicitly we have made use of the fact that the average orientation between dipoles two and one is independent of θ_r. The relative angles η and ψ defined in Eq. (3.16) are applicable here, and with Eqs. (3.16)–(3.19) the integration over angles in Eq. (B1) becomes

$$\begin{aligned}\ln G^s_{\text{st,uni}}(\mu) = \frac{c_2}{\lambda v^2}\int_0^1\int_0^1 [1 - e^{-q(x,y)} \\ - q(x,y)^{1/3}\gamma(\tfrac{2}{3},q(x,y))]\,dx\,dy\,,\end{aligned} \tag{B2}$$

where μ is defined in Eq. (4.6) and

$$q = \mu x^2(1+3y^2)\,. \tag{B3}$$

If, however, the exciting light is polarized along the z axis, normal to the planes, an initial distribution of excited molecules is produced which is proportional to $\cos^2\theta_0$. In consequence, the axial symmetry around the vector $\mathbf{r}$ is broken, which makes the use of the angles η and ψ obsolete. We can nevertheless restore the required symmetry by splitting up the electric field vector $\mathbf{E}$ in a radial component E_r, parallel to $\mathbf{r}$ and the angular part $E_{\theta r}$, perpendicular to $\mathbf{r}$. It is then

$$E_r = E\cos\theta_r\,, \tag{B4a}$$

$$E_{\theta r} = E\sin\theta_r\,. \tag{B4b}$$

Both field components can be thought of as exciting two independent orthogonal $\cos^2$ distributions which we recognize to be the distributions w_{0p} and w_{0n} encountered in Appendix A. In analogy to Appendix A we thus have to evaluate the averages $\bar{f}_p$ and $\bar{f}_n$ and weight them with $\cos^2\theta_r$ and $\sin^2\theta_r$, respectively [Eq. (B4)] as we later perform the integration over θ_r.

As before, $\bar{f}_n$ is obtained from

$$\bar{f}_n = \tfrac{1}{2}(3\langle f\rangle_{\text{uni}} - \bar{f}_p)\,. \tag{B5}$$

The angular average $\bar{f}_z$ between an initial distribution in layer one excited by z-polarized light and an isotropic distribution in layer two, at the fixed relative position defined by θ_r, ϕ_r is therefore

$$\bar{f}_z(\theta_r) = \cos^2\theta_r \bar{f}_p + \sin^2\theta_r \bar{f}_n . \tag{B6}$$

Using Eq. (B5) we obtain from Eq. (B6),

$$\bar{f}_z(\theta_r) = \bar{f}_p(\tfrac{3}{2}\cos^2\theta_r - \tfrac{1}{2}) + \langle f\rangle_{\text{uni}}(\tfrac{3}{2} - \tfrac{3}{2}\cos^2\theta_r) . \tag{B7}$$

We now replace f by $(1 - e^{-q\cos^6\theta_r})$ [see Eqs. (2.12) and (B3)] and explicitly calculate the angular averages $\bar{f}_p$ and $\bar{f}_{\text{uni}}$:

$$\begin{aligned}\bar{f}_z(\theta_r) &= \int_0^1\int_0^1 (1 - e^{-q(x,y)\cos^6\theta_r})(\tfrac{3}{2}\cos^2\theta_r - \tfrac{1}{2})3\cdot y^2\,dx\,dy \\ &\quad + \int_0^1\int_0^1 (1 - e^{-q(x,y)\cos^6\theta_r})(\tfrac{3}{2} - \tfrac{3}{2}\cos^2\theta_r)\,dx\,dy .\end{aligned} \tag{B8}$$

The factor $3y^2$ in the first integral of Eq. (B8) is the normalized distribution $w_{0p} = 3\cos^2\eta$.

Finally we integrate Eq. (B8) over θ_r and ϕ_r using Eq. (4.2) and obtain after rearranging the terms:

$$\begin{aligned}\ln G^s_{\text{st},z}(\mu) = &-\frac{3c_2}{\lambda v^2}\int_0^{\pi/2}\int_0^1\int_0^1 (1 - e^{-q(x,y)\cos^6\theta_r}) \\ &\times(1-y^2)\frac{\sin\theta_r}{\cos^3\theta_r}\,d\theta_r\,dx\,dy \\ &-\frac{3c_2}{\lambda v^2}\int_0^{\pi/2}\int_0^1\int_0^1 (1 - e^{-q(x,y)\cos^6\theta_r}) \\ &\times(3y^2-1)\frac{\sin\theta_r}{\cos\theta_r}\,d\theta_r\,dx\,dy .\end{aligned} \tag{B9}$$

With the substitution

$$s = q(x,y)\cos^6\theta_r \tag{B10}$$

we can simplify to

$$\begin{aligned}\ln G^s_{\text{st},z}(\mu) = &-\frac{c_2}{2\lambda v^2}\int_0^{q(x,y)}\int_0^1\int_0^1 q(x,y)^{1/3} \\ &\times(1-e^{-s})\,s^{-4/3}(1-y^2)\,ds\,dx\,dy \\ &-\frac{c_2}{2\lambda v^2}\int_0^{q(x,y)}\int_0^1\int_0^1 (1-e^{-s}) \\ &\times s^{-1}(3y^2-1)\,ds\,dx\,dy .\end{aligned} \tag{B11}$$

Integration over s can be performed analytically [see Eqs. (4.9)–(4.12) for the first integral in Eq. (B11) and Ref. 35 for the second one]:

$$\begin{aligned}\ln G^s_{\text{st},z}(\mu) = &\frac{3c_2}{2\lambda v^2}\int_0^1\int_0^1 [1 - e^{-q(x,y)} \\ &- q(x,y)^{1/3}\gamma(\tfrac{2}{3},q(x,y))](1-y^2)\,dx\,dy \\ &+\frac{c_2}{2\lambda v^2}\int_0^1\int_0^1\sum_{k=1}^{\infty}(-1)^k\frac{q(x,y)^k}{k\cdot k!} \\ &\times(3y^2-1)\,dx\,dy .\end{aligned} \tag{B12}$$

The remaining dual integration is done numerically.

To obtain the asymptotic form for $\mu \ll 1$ we expand the exponential term in Eq. (B11) to first order; the result of the integration is

$$\ln G^s_{\text{st},z}(t) = -\tfrac{3}{5}c_2 v^4\frac{t}{\tau}, \quad \mu < 0.05 . \tag{B13}$$

The same procedure leads to

$$\ln G^s_{\text{st,uni}}(t) = -\tfrac{1}{2}c_2 v^4\frac{t}{\tau}, \quad \mu < 0.05 \tag{B14}$$

for the uniform excitation which is identical to the dynamic situation, Eq. (4.14).

The asymptotic form for large values of μ is found by neglecting the exponential terms in Eq. (B12) and approximating $\gamma(2/3,q)$ and $\Sigma_{k=1}^{\infty}(-1)^k q^k/k\cdot k!$ by $\Gamma(\frac{2}{3})$ and $-C - \ln q$, respectively [Eq. (4.21)], where C is Euler's constant.

After integration one obtains

$$\ln G^s_{\text{st},z}(\mu) = \frac{c_2}{\lambda v^2}(0.6255 - 0.9356\,\mu^{1/3}) . \tag{B15}$$

Empirically it is found that the form

$$\ln G^s_{\text{st},z}(\mu) = \frac{c_2}{\lambda v^2}(0.8 - 0.9356\,\mu^{1/3}), \quad \mu > 500 , \tag{B16}$$

is the better approximation. The reason for the discrepancy in the offset parameter is that for the few orientations where q is still small the approximation $-C - \ln q$ is no longer valid and leads to contributions to the overall integral which are too large as compared to the exact sum expression, thus resulting in a negative bias.

Under uniform excitation conditions we obtain from Eq. (B2), using the same approximations as above:

$$\begin{aligned}\ln G^s_{\text{st,uni}}(\mu) &= \frac{c_2}{\lambda v^2}(1 - \langle|\kappa|^{2/3}\rangle_{\text{uni}}\cdot\Gamma(\tfrac{2}{3})\,\mu^{1/3}) \\ &= \frac{c_2}{\lambda v^2}(1 - 1.0016\,\mu^{1/3}) .\end{aligned} \tag{B17}$$

It can easily be shown that as the two layers are brought infinitely close together, Eqs. (B15) and (B17) transform into the monolayer expressions [Eq. (3.10) and Appendix A].

APPENDIX C

In this section we derive the asymptotic forms of Eqs. (4.33) and (4.37) and show an alternative way to numerically evaluate the integral [Eq. (4.33)]. In order to circumvent the singularity at $s = 0$ when numerically integrating Eq. (4.33), two successive partial integrations can be performed to leave only terms of the form

$$H(\alpha) = \int_0^1 \exp[-\mu(\langle a_1\rangle s - \langle a_2\rangle s^{4/3} + \langle a_3\rangle s^{5/3})]\cdot s^{\alpha}\,ds \tag{C1}$$

with $\alpha \geq 0$, whose numerical evaluation is safer. Equation (4.33) thus becomes

$$\ln G_d^s(\mu) = \frac{c_2}{\lambda v^2}\{1 - (1 + \tfrac{3}{2}\mu\langle a_1\rangle)\exp[-\mu(\langle a_1\rangle - \langle a_2\rangle + \langle a_3\rangle] + \mu[\tfrac{4}{3}\langle a_2\rangle H(0) - \tfrac{5}{3}\langle a_3\rangle H(\tfrac{1}{3})]$$

$$+\mu^2[-\tfrac{3}{2}\langle a_1\rangle^2 H(\tfrac{2}{3}) + 2\langle a_1\rangle\langle a_2\rangle H(1) - \tfrac{5}{3}\langle a_1\rangle\langle a_3\rangle H(\tfrac{4}{3})]\}. \quad \text{(C2)}$$

The asymptotic form for small values of μ is found again by using the first order power series of the integrand in Eq. (4.33):

$$\ln G_d^s(t) = -\frac{c_2}{\lambda v^2}\mu(\langle a_1\rangle/2 - \langle a_2\rangle/3 + \langle a_3\rangle/4)$$

$$= -\tfrac{9}{32}c_2\frac{t}{\tau}v^4 \quad \text{for } \mu < 0.05. \quad \text{(C3)}$$

To find the asymptotic form for large values of μ we rewrite Eq. (4.33) with the substitution

$$z = \langle a_1\rangle \mu s, \quad \text{(C4)}$$

$$\ln G_d^s(\mu) = -\frac{c_2}{3\lambda v^2}(\langle a_1\rangle\mu)^{1/3}\int_0^{\langle a_1\rangle\mu}\Bigg[1 - e^{-z} \cdot \exp\Bigg(\frac{\langle a_2\rangle}{\langle a_1\rangle^{4/3}}\cdot\frac{z^{4/3}}{\mu^{1/3}} - \frac{\langle a_3\rangle}{\langle a_1\rangle^{5/3}}\cdot\frac{z^{5/3}}{\mu^{2/3}}\Bigg)\Bigg]\cdot z^{-4/3}\,dz. \quad \text{(C5)}$$

If $\mu \gg 1$, the major contribution to the integral [Eq. (C5)] is in the range $z \ll \mu$ because this part is strongly weighted by $z^{-4/3}$. Yet, in this same region, the argument of the second exponential term is small so that we can proceed to approximate it to first order which leads to

$$\ln G_d^s(\mu) = -\frac{c_2}{3\lambda v^2}\Bigg[(\langle a_1\rangle_\mu)^{1/3}\int_0^{\langle a_1\rangle\mu}(1 - e^{-z})z^{-4/3}\,dz - \frac{\langle a_2\rangle}{\langle a_1\rangle}\int_0^{\langle a_1\rangle\mu}e^{-z}\,dz + \frac{\langle a_3\rangle}{\langle a_1\rangle}(\langle a_1\rangle\mu)^{-1/3} \times \int_0^{\langle a_1\rangle\mu}e^{-z}z^{1/3}\,dz\Bigg]. \quad \text{(C6)}$$

Any incomplete gamma functions which are obtained after integrating Eq. (C6) are well approximated by complete ones so that the asymptotic form becomes

$$\ln G_d^s(\mu) = \frac{c_2}{\lambda v^2}\Bigg[1 + \frac{\langle a_2\rangle}{3\langle a_1\rangle} - (\langle a_1\rangle\mu)^{1/3}\Gamma(\tfrac{2}{3}) - \frac{\langle a_3\rangle}{9\langle a_1\rangle}(\langle a_1\rangle\mu)^{-1/3}\Gamma(\tfrac{1}{3})\Bigg]$$

$$= \frac{c_2}{\lambda v^2}[1.8 - 1.4587\mu^{1/3} - 0.4974\mu^{-1/3}]. \quad \text{(C7)}$$

Its validity has been established for $\mu > 5000$. In the limit of μ going to infinity the monolayer expression is retrieved [Eq. (3.8)]:

$$\lim_{\mu\to\infty}\ln G_d^s(\mu) = -c_2\lambda^{-2/3}(\tfrac{3}{2}\langle a_1\rangle)^{1/3}\Gamma(\tfrac{2}{3})\left(\frac{t}{\tau}\right)^{1/3}. \quad \text{(C8)}$$

The asymptotic forms for transfer in the static limit follow from Eq. (4.37) by applying the same approximations as in the dynamic treatment. Consequently, the result for small values of μ is found to be identical to Eq. (C3). For large μ, however, the asymptotic form cannot be formally established using the arguments following Eq. (C5) because there exist relative orientations where a_1 is very small, and the assumptions which were used are no longer valid for these few orientations. Nevertheless, it is found that the functional form [Eq. (C7)] is conserved, $\langle a_1\rangle^{1/3}$ transforms to $\langle a_1^{1/3}\rangle$ and the coefficients k_1 and k_2 can be determined empirically by fitting to the exact form Eq. (4.37):

$$\ln G_{st}^s(\mu) = \frac{c_2}{\lambda v^2}(k_1 - \langle a_1^{1/3}\rangle\,\Gamma(\tfrac{2}{3})\,\mu^{1/3} - k_2\,\Gamma(\tfrac{1}{3})\,\mu^{-1/3}) \quad \text{(C9)}$$

with

$$k_1 = 1.6,$$

$$k_2 = -0.5,$$

which gives

$$\ln G_{st}^s(\mu) = \frac{c_2}{\lambda v^2}(1.6 - 1.2813\,\mu^{1/3} + 1.34\,\mu^{-1/3}) \quad \text{for } \mu > 5000. \quad \text{(C10)}$$

[1] Th. Förster, Ann. Phys. (Leipzig) **2**, 55 (1948).
[2] Th. Förster, Z. Naturforsch. Teil A **4**, 321 (1949).
[3] Th. Förster, Z. Elektrochem. **64**, 157 (1960).
[4] K. Sauer, Acc. Chem. Res. **11**, 257 (1978).
[5] D. L. Dexter, J. Chem. Phys. **21**, 836 (1953).
[6] St. W. Haan and R. Zwanzig, J. Chem. Phys. **68**, 1879 (1978).
[7] C. R. Gochanour, H. C. Andersen, and M. D. Fayer, J. Chem. Phys. **70**, 4254 (1979).
[8] C. R. Gochanour and M. D. Fayer, J. Phys. Chem. **85**, 1989 (1981).
[9] R. F. Loring, H. C. Andersen, and M. D. Fayer, J. Chem. Phys. **76**, 2015 (1982).
[10] R. J. D. Miller, M. Pierre, and M. D. Fayer, J. Chem. Phys. **78**, 5138 (1983).
[11] R. F. Loring and M. D. Fayer, Chem. Phys. **70**, 139 (1982).
[12] M. D. Ediger and M. D. Fayer, J. Chem. Phys. **78**, 2518 (1983).
[13] M. D. Ediger, R. P. Domingue, and M. D. Fayer, J. Chem. Phys. **80**, 1246 (1984).
[14] M. D. Ediger and M. D. Fayer, Macromolecules **16**, 1839 (1983); G. H. Fredrickson, H. C. Andersen, and C. W. Frank, *ibid.* **17**, 54 (1984).
[15] M. D. Ediger, R. P. Domingue, K. A. Peterson, and M. D. Fayer, Macromolecules **18**, 1182 (1985) and references therein.
[16] S. G. Fedorenko and A. I. Burshtein, Chem. Phys. **98**, 341 (1985).
[17] D. L. Huber, D. S. Hamilton, and B. Barnett, Phys. Rev. B **16**, 4642 (1977); W. Y. Ching, D. L. Huber, and B. Barnett, *ibid.* **17**, 5025 (1978).
[18] A. Blumen and J. Manz, J. Chem. Phys. **71**, 4694 (1979).
[19] T. N. Estep and T. E. Thompson, Biophys. J. **26**, 195 (1979); B. Kwok-Keung Fung and L. Stryer, Biochemistry **17**, 5241 (1978).
[20] W. E. Blumberg, in *Physical Methods on Biological Membranes and Their Model Systems*, edited by F. Conti, W. E. Blumberg, I. de Gier, and F.

Pocchiari, NATO ASI Series (Plenum, New York, 1985), p. 95.
[21]J. Knoester and J. E. van Himbergen, J. Chem. Phys. **81**, 4380 (1984).
[22]A. Blumen, J. Chem. Phys. **74**, 6926 (1981).
[23]G. H. Fredrickson and C. W. Frank, Macromolecules **16**, 1198 (1983).
[24]I. Z. Steinberg, J. Chem. Phys. **48**, 2411 (1968).
[25]H. Kellerer and A. Blumen, Biophys. J. **46**, 1 (1984).
[26]J. Yguerabide and L. Stryer, Proc. Natl. Acad. Sci. USA **68**, 1217 (1971).
[27]D. Axelrod, Biophys. J. **26**, 557 (1979).
[28]M. Hauser, U. K. A. Klein, and U. Gösele, Z. Phys. Chem. NF **101**, 255 (1976).
[29]J. Knoester and J. E. van Himbergen, J. Chem. Phys. **80**, 4200 (1984).
[30]H. Kuhn, D. Möbius, and H. Bücher, in *Physical Methods of Chemistry, Part IIIB*, edited by Weissberger and Rossiter, Techniques of Chemistry, Vol. I (Wiley Interscience, New York, 1972), p. 577.
[31]K. Kemnitz, T. Murao, I. Yamazaki, N. Nakashima, and K. Yoshihara, Chem. Phys. Lett. **101**, 337 (1983); F. Willig, A. Blumen, and G. Zumofen, *ibid.* **108**, 222 (1984); Ph. Anfinrud, R. L. Crackel, and W. S. Struve, J. Phys. Chem. **88**, 5873 (1984); Y. Liang and A. M. Ponte Goncalves, *ibid.* **89**, 3290 (1985).
[32]Ph. A. Anfinrud, D. E. Hart, J. F. Hedstrom, and W. S. Struve (to be published).
[33]H. Bücher, K. H. Drexhage, M. Fleck, H. Kuhn, D. Möbius, F. P. Schäfer, J. Sondermann, W. Sperling, P. Tillmann, and J. Wiegand, Mol. Cryst. **2**, 199 (1967).
[34]C. R. Desper and I. Kimura, J. Appl. Phys. **38**, 4225 (1967).
[35]I. S. Gradshteyn and I. W. Ryzhik, *Tables of Integrals, Series and Products* (Academic, New York, 1965).
[36]K. H. Drexhage, M. M. Zwick, and H. Kuhn, Ber. Bunsenges. **67**, 62 (1963).
[37]J. Klafter and A. Blumen, J. Lumin. **34**, 77 (1985).
[38]B. Mandelbrot, *The Fractal Geometry of Nature* (Freeman, San Francisco, 1982).
[39]C. L. Yang, P. Evesque, and M. A. El-Sayed, J. Phys. Chem. **89**, 3442 (1985).
[40]M. D. Galanin, Tr. Fiz. Inst. Akad. Nauk. USSR **5**, 341 (1950).
[41]F. W. Craver and R. S. Knox, Mol. Phys. **22**, 385 (1971).
[42]A. Jablonski, Acta Phys. Polon. A **38**, 453 (1970).
[43]G. Eyring and M. D. Fayer, J. Chem. Phys. **81**, 4314 (1984).